Stratigraphy in the Greenland/ Iceland/Norwegian (GIN) seas: A multiproxy approach on Pleistocene sediments

Marjolaine E J Sabine, Frédérique Eynaud, Sébastien Zaragosi, Jacques Giraudeau, Maxime Debret, Linda Rossignol-Malaize, Karine Charlier, Isabelle Billy, Bruno Malaize, Jimmy Daynac, et al.

Stratigraphy in the Greenland/Iceland/Norwegian (GIN) seas: A multiproxy approach on Pleistocene sediments

Marjolaine E.J. Sabine[a], Frédérique Eynaud[a, *], Sébastien Zaragosi[a], Jacques Giraudeau[a], Maxime Debret[b], Linda Rossignol-Malaize[a], Karine Charlier[a], Isabelle Billy[a], Bruno Malaize[a], Jimmy Daynac[a], Elodie Marches[c], Thierry Garlan[c]

[a] Laboratoire Environnements et Paléoenvironnements Océaniques et Continentaux (EPOC)—UMR CNRS 5805, Université de Bordeaux, Pessac, France
[b] Département de Géosciences et Environnement—Morphodynamique Continentale et Côtière, Sciences et Techniques, Université de Rouen, Mont-Saint-Aignan, France
[c] Service hydrographique et océanographique de la Marine (SHOM), Brest, France
*Corresponding author: e-mail address: frederique.eynaud@u-bordeaux.fr

Abstract

A multiproxy sedimentological study was conducted on five sediment cores retrieved between 67 and 79°N in the Greenland/Iceland/Norwegian seas in order to infer a common chronostratigraphic model for the selected cores. This model is based on the use of a series of geochemical, physical and micropaleontological proxies which are routinely measured in sedimentological investigations of marine sediment cores: the major and minor element content derived from X-Ray Fluorescence (XRF) core scanner analyses; the lightness and color of the sediment derived from spectrophotometry analyses; the magnetic susceptibility of the sediment; the distribution of planktonic foraminiferal assemblages combined to coccolith stratigraphy (acme zones) providing preliminary stratigraphic tie points. All those proxies are correlated independently between the five sediment cores. Our results demonstrate that high resolution studies using those standard paleoceanographical tools are powerful for establishing core-to-core correlation. A chronostratigraphical framework is proposed based on the correlation of the planktonic $\delta^{18}O$ isotopic record obtained in core M17KC03 with the LR04 benthic $\delta^{18}O$ reference stack. A comparison between the M17KC03 stratigraphy and other dated cores from the sub-polar North Atlantic confirms the robustness of the approach. Our study suggests that XRF core scanner-derived elemental ratios (especially those related to Ca), the lightness L* and the coccolith-based biostratigraphy provide robust stratigraphic tie-points at the scale of the whole Greenland/Iceland/Norwegian seas. The elemental ratio Sr/sum, the magnetic

Stratigraphy & Timescales
ISBN 2468-5178
https://doi.org/10.1016/bs.sats.2022.09.004

susceptibility, and planktonic foraminiferal records have a more local stratigraphic significance in the GIN seas. Over the last 1100 ka BP, our datasets are indicative of: (1) an excursion of Ca content and planktonic foraminiferal abundances during MIS 11, (2) an overall decrease toward present of both the detrital content (with the exception of values characterizing MIS 12) and of the magnetic susceptibility of sediments deposited during Glacials.

Highlights

Multiproxy approach for a robust stratigraphy in the Nordic seas.
New Pleistocene subboreal records.
Sedimentological expression of marine isotopic stages.

1. Introduction

Stratigraphy is the backbone of every marine sedimentological investigation during the Pleistocene where glacial and interglacial climate shifts paced paleoceanographic changes. In the northernmost basins of the North Atlantic (NAtl), i.e., the Greenland/Iceland/Norwegian (GIN) seas, the alternation of glacial and interglacial periods at the orbital scale drives drastic environmental shifts and readjustments, those seas moving from cold-polar to milder-subpolar climates at both extremes. The GIN seas also constitute a crucial component of the Atlantic Meridional Overturning Circulation (AMOC), and thus conversely can drive global climatic changes (e.g., Becker et al., 2018; Chauhan et al., 2014; Müller and Stein, 2014; Thibodeau et al., 2017). Despite contrasted contexts registered between glacials and interglacials, the establishment of a robust stratigraphy is still a prime challenge in those seas, with the main limitations being attributed to: (1) meager sedimentation rates (1–3 cm/ka out of the channels and troughs, e.g., Laberg et al., 2000), (2) the microfossils scarcity and (3) strongly variable oceanographic conditions in these strongly reactive areas. Indeed, climatic changes impact on diverse components of this complex oceanographic system: e.g., on the thickness and lateral extension of the surrounding ice-sheets, the sea-level, the sea-ice cover extension and duration, the water column structure and dynamics (including the pathway of currents, deep, intermediate and surface as well), and also the photic zone thickness (e.g., Andrews, 2000; Blind-

heim et al., 2000; Broecker et al., 1990; Rahmstorf, 1999, 2002, 2013; Samtleben et al., 1995; Sejrup et al., 2011). Those subpolar seas are additionally strongly affected by the dissolution of pelagic carbonates, with the lysocline (or Carbonate Compensation Depth—CCD) which can be very close to the surface according to regional environmental and climatic conditions (e.g., Huber et al., 2000 and references therein; Henrich et al., 2002). The sediment cores from the GIN seas thus generally present several intervals of calcareous microfossils-free sediments (Bylinskaya et al., 2016; Chauhan et al., 2016; this study). This total absence might be explained by specific environmental conditions (such as a perennial sea-ice cover or cold and fresh surface currents over the studied area, e.g., Huber et al., 2000), or by a substantial dissolution (at the bottom by post-depositional dissolution or in the whole water column). The influence of variable sea-surface conditions, with seasonally driven freshwater advection, melting ice and/or sea-ice and brine rejection, can also modify the water $\delta^{18}O$ ratio and, in consequences, the foraminifera test chemical composition, making difficult the use of the $\delta^{18}O$ solely to construct a reliable stratigraphic scale (e.g., Hillaire-Marcel and de Vernal, 2008; Rohling, 2013). In consequence, paleoceanographic works conducted in the GIN seas with stratigraphies exceeding the ^{14}C measuring limits are hampered by all these limitations, and published ages can be questionable. However, thanks to the recovery of long marine archives over the last five decades, some coherent protocols have emerged crossing multiproxy data to refine age scales at their most reliable possible degree (e.g., Caricchi et al., 2020; Channell and Hodell, 2013; Chapman and Shackleton, 1998; Helmke et al., 2002; Hodell et al., 2008, 2015; Lucchi, 2013; Martrat et al., 2014). These studies provide relevant and widely used tools for stratigraphic correlation and dating, giving much more comprehensive palaeoclimatic studies, especially regarding the coupling between the ocean and other reservoirs (e.g., Clark et al., 2006). Actually, those dating protocols give access to reservoir phasing or dephasing and to the processes and feedbacks involved in such environmental dynamics at orbital scales. In the NAtl, a consensus exists regarding the sedimentary typicity of interglacials (and conversely glacials) with high carbonate contents (associated to high contents of calcareous microfossils and whiter sediments), low terrigenous supplies (ice-rafted debris -IRD included) and low stable isotopic benthic oxygen ratio occurring at that times and defining plateau during

warmth optima (e.g., Bauch et al., 2000; Bylinskaya et al., 2016; Knies et al., 2009).

This study was conducted on a series of new long marine cores with the aim to further document the paleoceanographical history of the GIN seas in a consolidated stratigraphical approach, taking into account a panel of selected proxies (in complement to the classical $\delta^{18}O$ tool) providing the possibility of robust core correlations over the studied region. With this article, we finally conceptualize a practical tutorial to use as a paleoclimatic and stratigraphic guideline in these sub-boreal domains. This work is based on five sediment cores retrieved in 2017 during the MOCOSED cruise on the R/V *Pourquoi Pas*?, and on reference archives from the subpolar NAtl. The MOCOSED 2017 cores were selected because of their geographical position along contrasted contexts of the GIN seas, in order to illustrate and construct a coherent regional scenario of climate induced changes in those basins. Also, their distant position from the surrounding trough mouth fans (i.e., TMF, which can have an average sedimentation rate much higher, until 400 cm/ka according to, e.g., Baeten et al., 2014) gives more chance to register the most possible prolonged time scale. The analyses were performed following the same methodological protocol in order to obtain comparable datasets to be crossed core by core. The following paragraphs: (1) detail our approach and discuss its suitability to address stratigraphical problems classically met by paleoceanographers in the subboreal and boreal realms; and (2) discuss time intervals that our study recovers in the GIN seas at the light of other long records retrieved in this basin but also in the NAtl.

2. Materials, methods and proxy significance

Five sediment cores (Fig. 1, Table 1) were retrieved with a CALYPSO piston corer on the R/V *Pourquoi Pas?* during the MOCOSED cruise in September 2017. Cores M17KC01, M17KC02, and M17KC03 were retrieved from the southern GIN seas (south of Jan Mayen Fracture Zone) in the Norwegian/Icelandic seas. They were selected based on subsurface seismic CHIRP data which indicated a sediment stacking assuming the possibility of collecting a long time series. Cores M17KC15 and M17KC14 were retrieved from the central Fram Strait, in the northern GIN seas, this area being at the transition between the arctic ocean and

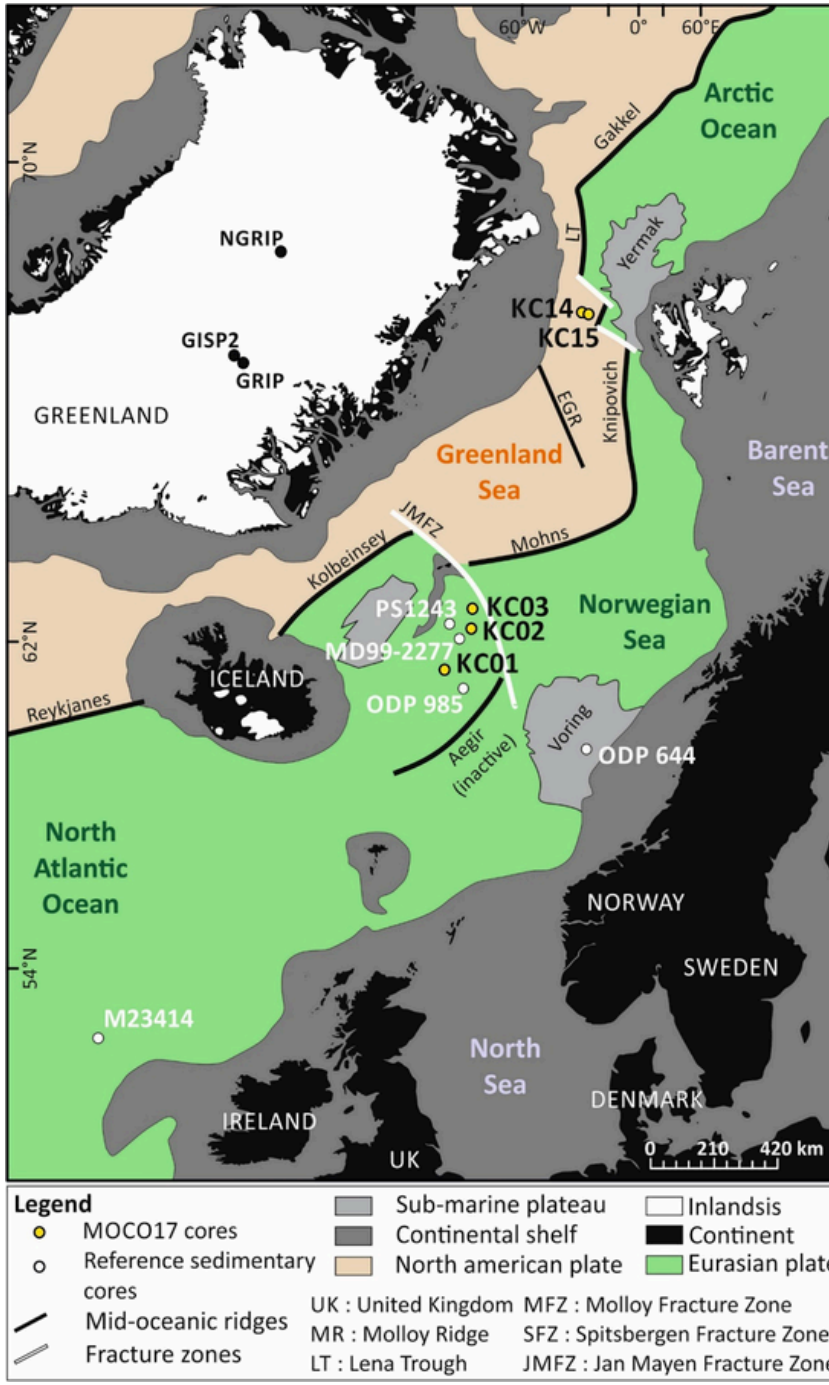
60°W
0°
60°E
70°N
62°N
54°N
Arctic Ocean
Gakkel
LT
Yermak
NGRIP
GISP2
GRIP
GREENLAND
KC14
KC15
EGR
Knipovich
Barents Sea
Greenland Sea
JMFZ
Kolbeinsey
Mohns
PS1243
KC03
KC02
MD99-2277
KC01
Norwegian Sea
ICELAND
Reykjanes
ODP 985
Aegir (inactive)
Voring
ODP 644
North Atlantic Ocean
NORWAY
SWEDEN
M23414
North Sea
DENMARK
IRELAND
UK
0 210 420 km
Legend
MOCO17 cores
Reference sedimentary cores
Mid-oceanic ridges
Fracture zones
Sub-marine plateau
Continental shelf
North american plate
Inlandsis
Continent
Eurasian plate
UK : United Kingdom
MR : Molloy Ridge
LT : Lena Trough
MFZ : Molloy Fracture Zone
SFZ : Spitsbergen Fracture Zone
JMFZ : Jan Mayen Fracture Zone

the GIN seas, which made it a key area to study the paleoclimatic changes.

2.1 Sedimentary analyses

The cores were cut in 1-m section on board, themselves divided into two half-sections, split lengthways. Each split section was analyzed with the spectrophotometer Minolta Cm-2600d UV-visible at a 1-cm step interval, with a 10 nm increment over the 360–740 nm bandwidth. The lightness (L*) scale from 0 to 100, can be compared to the gray-scale reflectance and can be used as a paleoclimatic indicator, as does the color a*, indicative of red-green color of the sediment (i.e., Chapman and Shackleton, 1998; Debret et al., 2011, see Table 2). Then, 1-cm-step magnetic susceptibility measurements were performed with a Barington MS2E.

Each split section was sampled by 7.5-cm-wide, 1-cm-thick aluminum plate in the central part of the section, giving slice of sediment. Then, sediment samples were collected from those aluminum plates (which minimize the effects of the core walls). They were analyzed for sedimentological characteristics and to determine their microfossil contents, focusing on coccolithophorids and planktonic and benthic foraminifera at *EPOC (Environnement et Paléoenvironnement Océaniques et Continentaux)* laboratory.

X-ray fluorescence (XRF) core-scan analyses were performed at a 1-cm-step resolution on each core, using an Avaatech instrument at 10 and 30 kV setting (*EPOC Laboratory PACS instruments: https://www.epoc.u-bordeaux.fr/index.php?lang=fr&page=pf_carottes)*. For the purpose of this study, the Ca, Ti, Mn, Sr, and Fe contents were especially identified as significant. The following thus shortly summarizes key information identified for each studied area (in accordance with what is known for these elements, see Table 2 and Supplementary information in the online version at https://doi.org/10.1016/bs.sats.2022.09.004 SI-1). The two southernmost cores, M17KC01 and M17KC02, present a prevalent calcium content in the sediment which is usually a marker of the calcareous primary production (e.g., Hodell et al., 2008; Richter et al., 2006). The M17KC03, near Jan Mayen fracture zone, shows iron as prevalent

Fig. 1 Physiographic map of the North Atlantic and location of marine cores and drillings studied and/or discussed in the text. (For interpretation of the references to color in the figure legends, the reader is referred to the Web version of this article.)

Table 1 List of the marine cores and of reference archives (deep-sea drillings; ice core) used in this study to build a coherent stratigraphy.

	Core	Type	Altitude (m)	Recovery/length (m)	Latitude N (decimal degrees)	Longitude E (decimal degrees)	Retrieved in:	Location
Reference cores	ODP site 644	sediment	−1227	238.4	66.667	4.567	1985	Voring basin
	ODP site 985	sediment	−2788	129.44	66.942	−6.450	1996	Northeastern Iceland Sea
	M23414	sediment	−2196	9.08	53.530	−17.000	1991	Rockall Plateau
	PS1243	sediment	−2721	7.67	69.380	−6.510	1984	Norwegian Sea
	MD99–2277	sediment	−2800	36.65	69.250	−6.321	1999	Jan Mayen Fracture Zone, Norwegian Sea
	MD01–2448	sediment	−3460	28.8	44.780	−11.275	2001	Bay of Biscay
	MD03–2705	sediment	−3000	37	18.097	−21.153	2003	Eastern Tropical Atlantic Ocean
	NGRIP	ice core	2917		71.500	−42.320	1999–2003	Center Greenland Ice Sheet
Studied cores	MOCO17-KC01	sediment	−2625	9.16	67.612	−6.659	2017	Norwegian Sea
	MOCO17-KC02	sediment	−3144	11.035	69.701	−5.079	2017	Jan Mayen Fracture Zone, Norwegian Sea

Core	Type	Altitude (m)	Recovery/length (m)	Latitude N (decimal degrees)	Longitude E (decimal degrees)	Retrieved in:	Location
MOCO17-KC03	Sediment	−2750	20.66	70.176	−5.240	2017	Jan Mayen Fracture Zone, Norwegian Sea
MOCO17-KC14	Sediment	−2674	9.17	79.215	−0.727	2017	Fram Strait
MOCO17-KC15	Sediment	−3095	8.46	79.334	0.591	2017	Fram Strait

Table 2 List of the sedimentary parameters/proxies used in this study with respect to their significance for stratigraphical purposes.

Parameters	State of art/Stratigraphical interpretation and usage	Key references	Threshold of interest in our study
Lightness L*	Lightness L* (Black/white variation) is the capacity of sediment to reflect the light. Light (/white) sediments traduce a high carbonate content and few dilution by the terrigenous components, they are attributed to warm climatic periods	Bauch et al. (2000), Chapman and Shackleton (1998), Debret et al. (2011)	Values >57 are usual during interglacials (*this study*)
Color a*	a* (red/green variation) is primarily controlled by the deposition of Fe and Mn-rich components, like red-colored hematite minerals	Helmke et al. (2002), Nagao and Nakashima (1992)	Low values can highly be correlated to iron in the sediment
^{XRF} Ca/sum ratio	Ca is part of marine carbonates but also derives from reworked carbonaceous material (depending upon the age of the weathered rocks)	Hodell et al. (2008), Kaboth-Bahr et al. (2019), Kolling and Bauch (2017), Rothwell and Croudace (2015), Richter et al. (2006)	Values >0.3 are usual during interglacials (*this study*)
^{XRF} Ti/Ca ratio	Ti is derived from continental rocks. In sediment, it is interpreted as a continental detrital material	Kaboth-Bahr et al. (2019), Richter et al. (2006), Rothwell and Croudace (2015)	Values <0.5 are linked to high planktonic content (*this study*)

Parameters	State of art/Stratigraphical interpretation and usage	Key references	Threshold of interest in our study
^{XRF} Mn/sum ratio	Mn follows glacial/ interglacial cyclicity in the central Artic ocean	Helmke et al. (2002), Jakobsson et al. (2000)	Values >0.01 are linked to deep-sea diamict (*this study*)
Absolute abundance of planktonic foraminifera (#/g)	High abundance of planktonic foraminifera implies favorable conditions for primary production and relatively warm and salty waters in the studied area	Bylinskaya et al. (2016), Chauhan et al. (2014)	Values >5 individual/g of dry sediment is usual during interglacials (*this study*)
Large Lithic Grains/LLG (#/g)	LLG correspond to sediment grains coarser than 1000 μm (independently of their morphology and nature)	Bauch et al. (2002), Bylinskaya et al. (2016)	Values >2 LLG/g of dry sediment is usual during glacials (*this study*)
% > 125 μm	Coarse sediments are usually interpreted as the result of strong current transport or drift-ice transport	Bauch et al. (2002), Bylinskaya et al. (2016)	Values >15% are usual during interglacials in the SOUTHERN GIN seas // Values >10% are usual during glacials in the NORTHERN GIN seas (*this study*)

Parameters	State of art/Stratigraphical interpretation and usage	Key references	Threshold of interest in our study
MS	The MS signal traduces the magnetic properties of sedimented particles: it depends of the magnetic source distance (advection from Iceland or other magnetic provinces for instance) and of the pathway of the currents which have played on sites. Its use in the Pleistocene sediments of the GIN seas has lead to the construction of north hemisphere reference stack (NAPIS)	Channell et al. (2003), (2009), Kissel et al. (1997), Kissel et al. (1999), Stoner et al. (2000), (2002)	–

element, followed by calcium. Then, in the two northernmost cores, M17KC14 and M17KC15, from the central Fram Strait, iron and silicon are prevalent in the sediment, as it is commonly observed in the Arctic Ocean (e.g., Stokes et al., 2005). In a recent study, Carbonara et al. (2016) used Ca/Ti ratio from a mid-depth sediment core from the Kveithola trough, southern Svalbard, to describe biogenic carbonate sedimentation. Consequently, they interpreted XRF calcium content as related to a biogenic content. This interpretation seems coherent with our results (see following sections). In that way, the Ca/sum ratio, with "sum" corresponding to the sum of all the elements registered during the measurements for each level, are interpreted as mainly signing calcareous biogenic materials. Strontium (Sr) is usually fixed by marine microorganisms at the same time as Ca, making this element an additional biogenic marker for the marine primary production specifically (e.g., Richter et al., 2006). Titanium (Ti) is prevalent in detrital material (Richter et al., 2006; Rothwell and Croudace, 2015) and is frequently used to identify terrigenous input (Carbonara et al., 2016). Manganese (Mn) is generally used to identify the climatic cyclicity in the central Arctic Ocean (e.g., Helmke et al., 2002; Jakobsson et al., 2000).

The cores are composed of alternated brown, light-gray and dark-gray muds bearing IRD, and silty to sandy laminated IRD-free muds. Grain-size analyses were performed through 4000 samples collected within the five sediment cores, with facies dependants selected intervals. The grain sizes were analyzed using a laser diffraction grain-size analyzer Malvern Mastersizer 2000.

2.2 Micropalaeontological analyses

The five sediment cores were sampled for micropalaeontological analyses taking into account the sedimentological facies changes with a 10 cm mean step, giving a total of 588 samples. Those sediment samples were dried in a heat chamber at 40 °C, weighed (average weight: 7.7 g), wet sieved using two sieves, 125 μm and 1000 μm. In polar basins, the 125 μm sieve is considered as keeping enough planktonic foraminifera being representative of the adult faunal assemblage. Within the GIN seas, each large lithic grain >1000 μm found in a clayey matrix is considered as brought to the deepest environments by glacial processes (sea-ice and iceberg loadings) (e.g., Amundsen et al., 2015; Haflidason et al., 2007). Those large lithic grains are thus interpreted as ice-rafted debris (IRD) in the following. The sieved material 125–1000 μm and >1000 μm was dried and weighed and the <125 μm sediment was not kept. The planktonic foraminifera were counted through the 125–1000 μm fraction and the IRD were counted through the >1000 μm fraction.

Coccolithophorids were used to establish a preliminary biostratigraphy based on their acme zones (coccolithophorid acme zones—CAZ) (Figs. 2 and 3A) (e.g., Pujos and Giraudeau, 1993; Wefer et al., 1998a). Sixty-three smears were collected and analyzed on the studied cores, without a regular sampling step but actually determined by lithological changes, according to sediment color and texture variation: ten smears were collected from the M17KC14, nine from the M17KC15, twenty-two from the M17KC03, thirteen from the M17KC02 and nine smears were collected from the M17KC01. The smears were observed under a standard light microscope with a magnification x1,000. The quantitative variations of different calcareous nannofossils species permit the identification of specific periods of time (Thierstein et al., 1977). Thus, Thierstein et al. (1977) describe *Pseudoemiliania lacunosa* disappearance after 450 ka BP, *Emiliania huxleyi* appearance 275 ka BP, and they determine dominance changes among *E. huxleyi* and *Gephyro-*

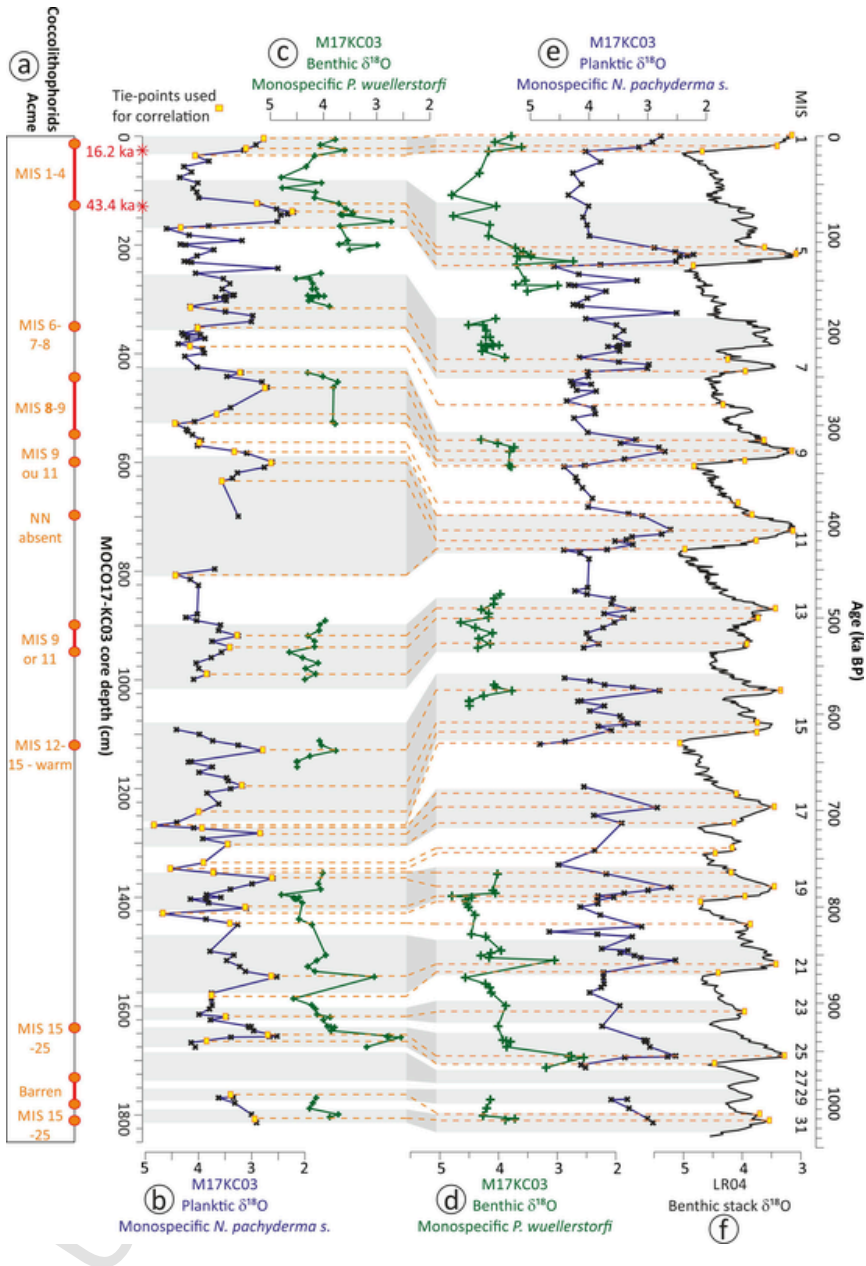

capsa caribbeanica in between 85 and 73 ka BP. The reference framework used in this work is the Neogene period's biostratigraphy defined by Wefer et al. (1998b) (Fig. 2).

Stable isotope ratios were measured on monospecific samples of foraminifera shells from the M17KC03 (benthic and planktonic) fossil assemblages. The measurements were done following standard laboratory techniques at the *EPOC Laboratory Isotopic Platform* with a Thermo Scientific Kiel IV Carbonate Device connected to a MAT253 isotope ratio mass spectrometer. All the measurements were calibrated on the Pee Dee Belemnite isotope standard (PDB). The $\delta^{18}O$ analytical precision is better than 0.08‰. The planktonic $\delta^{18}O$ signal has been obtained on monospecific samples of *Neogloboquadrina pachyderma* (*Nps*) using 8–16 specimens (selected from the 125–250 μm size). Because of the microfossils paucity, **only 161 (upon 251) samples contained planktonic foraminifera and have produced isotopic measurements** (Fig. 2B and E). The last two meters of sediment were totally free of calcareous microfossils.

$\delta^{18}O$ measurements were also performed on monospecific samples of the benthic species *Planulina wuellerstorfi* (selected from the 250–350 μm size). A + 0.64‰ correction factor was applied to *P. wuellerstorfi* $\delta^{18}O$ values, according to previous calibration studies (Duplessy et al., 1984; Shackleton and Opdyke, 1973). The microfossils scarcity limited the measurements to **only 100 (upon 251) samples** (Fig. 2C and D). Because of unexpected values, six points were double measured, the points 6, 56, 95, 157, 262 and 281 cm depth in the core. Each measurement was reproducible. However, the discontinuous specimen recovery over the core did not allowed us to produce a complete robust signal. Considering published works in the same area, we decided to follow approaches introduced by previous authors, i.e., to mainly rely on planktonic measurements for the construction of isotopic stratigraphic frameworks (see Bauch et al., 2000; Helmke and Bauch, 2002).

2.3 Data analytical procedures

Because the M17KC03 core (20.66 m long, southern GIN seas) recovers the temporally longest record, it was used as the reference core for our

Fig. 2 M17KC03 age model construction steps (deriving from $\delta^{18}O$ data correlated with the LR04 $\delta^{18}O$ benthic stack), with: (A) identified Coccolithophorids acme zones, (B) M17KC03 planktonic $\delta^{18}O$ (*Nps*) vs. core depth, (C) M17KC03 benthic $\delta^{18}O$ (*P. wuellerstorfi*) vs. core depth, (D) M17KC03 benthic $\delta^{18}O$ vs. age, (E) M17KC03 planktonic $\delta^{18}O$ vs. age, (F) $\delta^{18}O$ LR04 benthic stack (Lisiecki and Raymo, 2005).

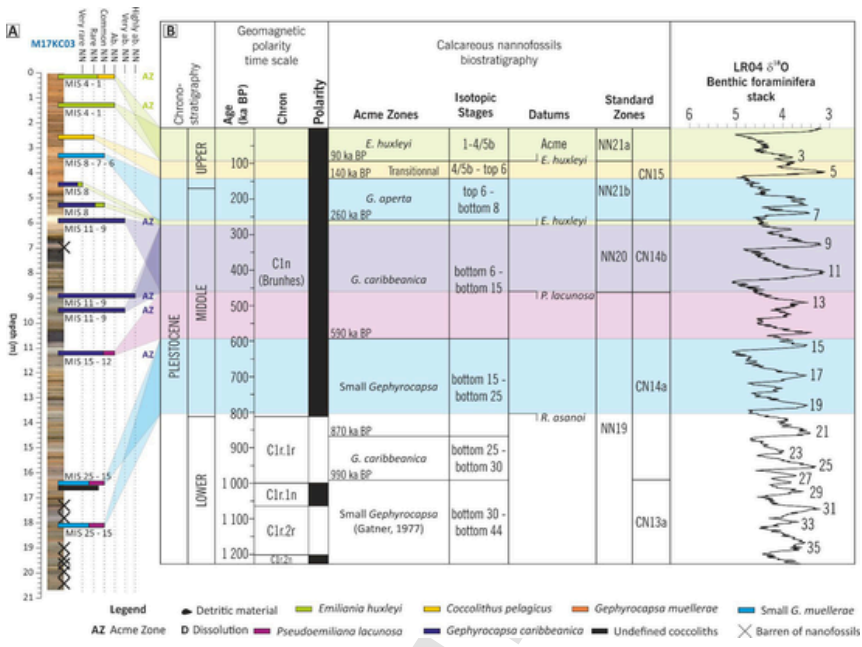

Fig. 3 M17KC03 nannofossil stratigraphy based on coccolithophorids acme zones. (A): identified coccolithophorids acme zones. (B): corresponding stratigraphy as defined by from Giraudeau et al. (1993) in the frame of the known chronostratigraphy, the geomagnetic polarity time scale, the calcareous nannofossil biostratigraphy and compared to the LR04 d18O benthic stack (Lisiecki and Raymo, 2005).

work. Then, with the AnalySeries software (Paillard et al., 1996), a core-to-core correlation was undertaken using a multiproxy method, fixing recurrent tie-points traceable in a maximum of cores. It facilitates the correlation of different graphical data (curves) peak-to-peak, and/or transition-to-transition, with the generation of tie-points. We considered scrupulously, all along the process, the stratigraphical framework defined by the CAZ (as illustrated in Fig. 2A and 3) as a basic timeline.

In complement, we conducted two radiocarbon datings on the reference core M17KC03 based on planktonic foraminifera shells. They were measured on monospecific samples of *Neogloboquadrina pachyderma* (sinistral)/*Nps* selected in the 125–1000 µm fraction (Table 3). Those datings were calibrated using the Calib 8.1.0 software, with the Marine 20 calibration set (Heaton et al., 2020; Stuiver and Reimer, 1993) and indicated into our correlations (Fig. 2) even if their coherency is disputable.

Table 3 Radiocarbon dates obtained from the M17KC03 sedimentary core.

Sample reference	Material	Depth (cm) in core	Laboratory number	Conventional radiocarbon age (a BP)	Error (yr)	Calibrated dates (cal a BP)/CALIB 8.1.0 Cal. Set: Marine 20		
						1 sigma ranges [sart:end] relative area	2 sigma ranges [sart:end] relative area	Mid age (a cal BP) 1 sigma
MOCO_KC03_26 cm (Ech 1)	Monospecific samples of *Neogloboquadrina pachyderma* (sinistral) form the 125–1000 μm fraction	26 cm	**Beta-529,357**	14,050	±40	[cal BP 16031: cal BP 16262] 1.	[cal BP 15912: cal BP 16386] 1	16,146.5
MOCO_Cc03_124 cm (Ech 2)		124 cm	**Beta-529,358**	41,210	±490	[cal BP 42981: cal BP 43821] 1.	[cal BP 42708: cal BP 44201] 1	43,401

Ages were calibrated with the CALIB 8.1.0 software (marine reservoir correction database Marine 20 after Stuiver and Reimer, 1993; Heaton et al., 2020).

3. Toward a coherent stratigraphy

3.1 Building the M17KC03 core stratigraphy

Our stratigraphy is based on a peak-to-peak correlation in between the M17KC03 *Nps* $\delta^{18}O$ record with the LR04 $\delta^{18}O$ benthic stack (Lisiecki et al., 2008; Lisiecki and Raymo, 2005). This correlation is shown on Fig. 2, both in depth (Fig. 2B and C) and age (Fig. 2D and F) to provide an objective view of the obtained tuning. Most of the $\delta^{18}O$ spikes correlate peak-by-peak to the glacial-interglacial interplay, reflecting the Marine Isotopic Stages 1 to 31.

Forty-one tie-points were needed for this correlation (Table 4, Figs. 2 and 4), taking into account the coherency with the CAZ obtained information (Fig. 3). This correlation, thus using independent microfossil tools, gives an age of around 1000 ka BP to the first 19 m of the M17KC03 sediment core.

According to this chronostratigraphy, the sedimentation rate values are low, around 3 cm/ka, except for the Marine Isotopic Stage (MIS) 11 record which is the thickest of the core, presenting a sedimentation rate of 19 cm/ka and for the MIS 16 which is almost absent (Fig. 4). The MIS 11 thickness explains the plateau observed on the age model (Fig. 4B). This anomaly strongly questioned our correlation at a first glance, but was constrained by the CAZ (Fig. 3). We consider the possibility of a *Pseudoemiliania lacunosa* disappearance occurring during the MIS 13 instead of the MIS 11 in the GIN seas, explaining the MIS 9–11 CAZ defined until 9.5 m depth in the sediment core (Pujos and Giraudeau, 1993; Thierstein et al., 1977).

To validate the obtained stratigraphy, the dated M17KC03 planktonic $\delta^{18}O$ was compared with the planktonic $\delta^{18}O$ record of the dated core PS1243 (the closest core) (Bauch et al., 2000), the planktonic $\delta^{18}O$ record of the ODP site 644 (Eldholm et al., 1987; Myhre and Eldholm, 1988), and the North GRIP $\delta^{18}O$ ice core data (Gkinis et al., 2014). Despite resolution differences, this comparison (Fig. 5) shows that the isotopic data measured on core M17KC03 are coherent with those records over the considered intervals. To go further, multiproxy data from the M17KC03 core, now put in age (Fig. 5A), have been compared with other datasets from those reference records when available

Table 4 Table listing the forty-one tie-points resulting from the correlation of the M17KC03 planktonic $\delta^{18}O$ record with the benthic $\delta^{18}O$ stacked record LR04 (Lisiecki and Raymo, 2005) using the Analyseries software.

Tie-points	M17KC03 Core-depth (cm from the top)	LR04 Age (ka BP)
1	6	0
2	24	11
3	37	17
4	124	116
5	140	123
6	170	135
7	317	232
8	353	245
9	388	280
10	436	316
11	463	328
12	512	337
13	529	343
14	564	381
15	583	394
16	601	411
17	635	420
18	810	430
19	919	491
20	942	501
21	990	528
22	1130	576
23	1196	610
24	1243	620
25	1268	631
26	1273	680
27	1282	697
28	1337	741
29	1365	780
30	1400	790
31	1403	800
32	1423	824
33	1547	856

Tie-points	M17KC03 Core-depth (cm from the top)	LR04 Age (ka BP)
34	1576	868

Tie-points	M17KC03 Core-depth (cm from the top)	LR04 Age (ka BP)
35	1617	890
36	1626	928
37	1654	954
38	1667	964
39	1769	1000
40	1785	1016
41	1807	1022

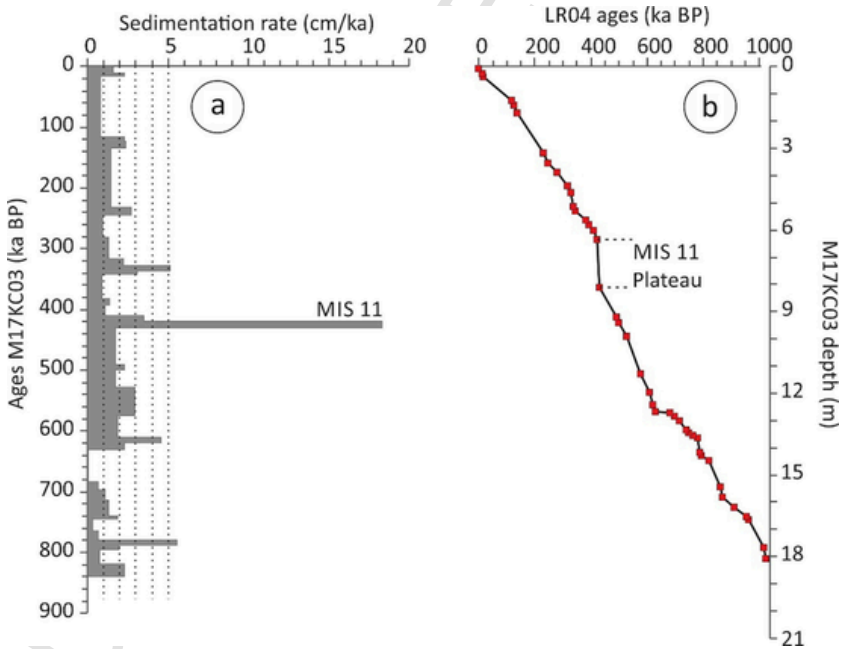

Fig. 4 M17KC03 constructed age model with the: (A) derived sedimentation rates in the core and (B) the tie graph between the M17KC03 signal and the LR04 scale.

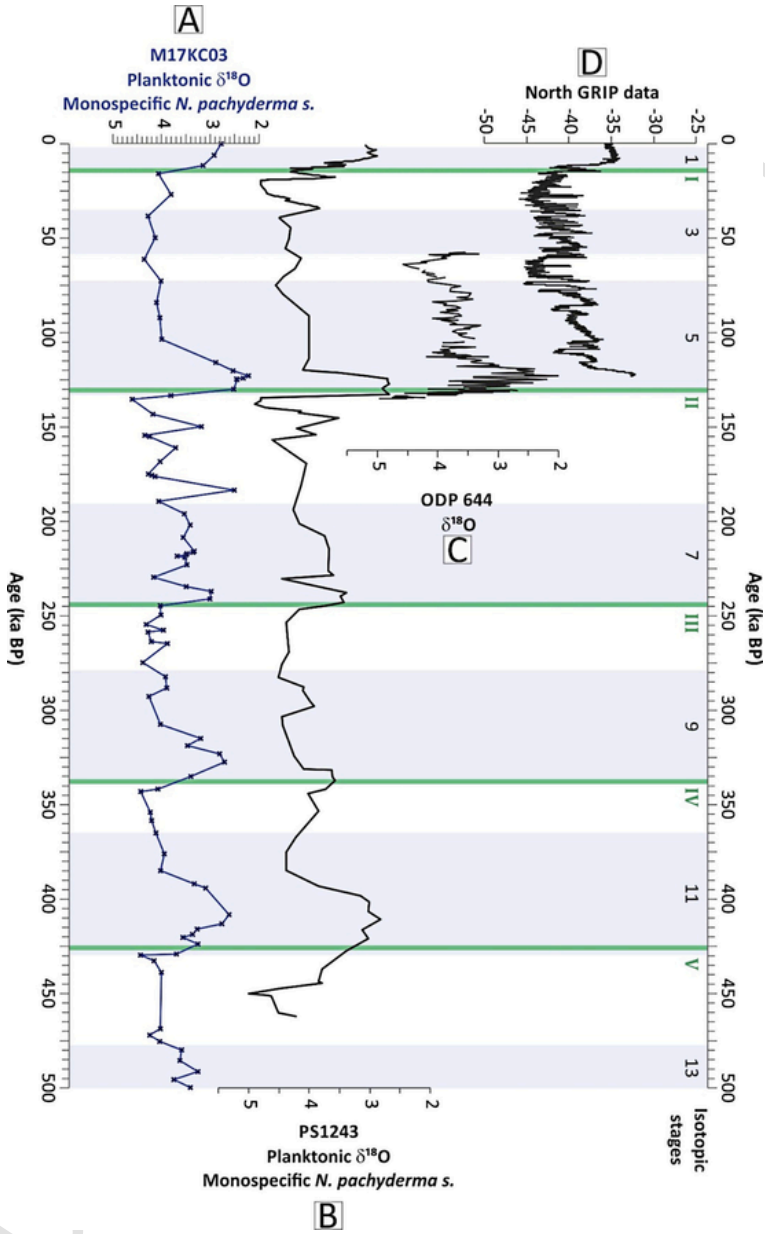

(Fig. 6). Unsurprisingly, the Ca/sum ratio correlates well with the benthic $\delta^{18}O$ stack LR04 (Fig. 6A) (Lisiecki and Raymo, 2005). A slight delay is however observed between interglacial peaks and Ca/sum ratio

peaks during some intervals. The Ca/sum ratio correlates also quite well with the ODP site 985 $CaCO_3$ (Fig. 6B) (Jansen et al., 1996) but a dephasing is observed before 400 ka BP. It can be explained by the fact that the chronostratigraphy of this latter record was established in 1999 by Raymo et al. on the basis of magnetostratigraphy and on dinocysts. Worth is noting that its thus shows also a delay with the more recent benthic $\delta^{18}O$ stack LR04 curve. The L* is impressively reproducible over more than 450 ka BP between the M17KC03 core and the PS1243 and M23414 sediment cores (Fig. 6C and D) (Bauch et al., 2000; Helmke et al., 2002). In the same way, the color a* is very well correlated between the M17KC03 and the PS1243 (Fig. 6E) (Bauch et al., 2000). **All those correlations taken together reinforce and give confidence to the approach we have chosen to construct the M17KC03 core stratigraphy**.

3.2 Core-to-core correlations (in depth) from the MOCOSED 2017 cruise

The six multiproxy parameters listed in Table 2 were used for the depth-to-depth correlations, generating 7 to 14 common tie-points (Table 5 and Fig. 7) between the studied cores. M17KC01 and M17KC02 (southern GIN seas) data are very similar to the M17KC03 core taken as a reference. M17KC14 and M17KC15 (northern GIN seas) show less similarity and three different parameters presented below (Figs. 8–10, other parameters are shown as Supplementary information in the online version at https://doi.org/10.1016/bs.sats.2022.09.004—Fig. SI-1 and SI-2) allowed us to produce a good correlation between the northern and southern GIN basins.

The first used parameter, the Ca/sum ratio, shows a very good match between the five sediment cores (Fig. 8). A very high peak of Ca/sum is identified around 5–7 m depth in the cores M17KC03, M17KC02, M17KC01, M17KC15 and around 9 m depth in the core M17KC14. The Coccolithophorids Acme Zones locate this positive excursion between

Fig. 5 (A) M17KC03 planktonic *Nps* $\delta^{18}O$ record in age, compared with: (B) the planktonic *Nps* $\delta^{18}O$ of the proximal PS1243 sediment core, and, for the last climatic cycle, with: (C) the planktonic $\delta^{18}O$ measurements of ODP site 644, and (D) the North GRIP glaciological $\delta^{18}O$ data (Bauch et al., 2000; Eldholm et al., 1987; Gkinis et al., 2014; Myhre and Eldholm, 1988).

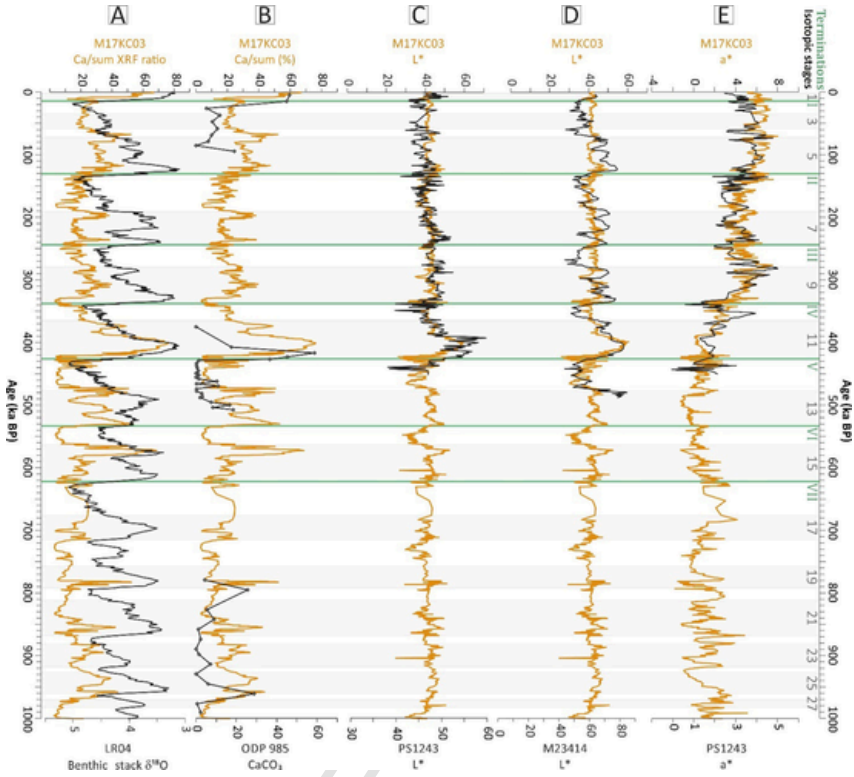

Fig. 6 Comparison of key data from reference cores identified in the vicinity of the GIN seas (black curves) with those of the studied core M17KC03 (orange curves). (A) ^{XRF}Ca/sum ratio in M17KC03 compared with the δ^{18}O LR04 benthic stack (Lisiecki and Raymo, 2005), (B) ^{XRF}Ca/sum ratio in M17KC03 compared with the equivalent carbonate concentration in the ODP site 985 (Raymo et al., 1999), (C) lightness parameter L* in M17KC03 and PS1243 (Bauch et al., 2000). (D) Lightness parameter L* in M17KC03 and M23414 (Bauch et al., 2000). (E) Color parameter a* in M17KC03 and PS1243 (Bauch et al., 2000). Note that we used comparable X scales to strengthen the correlations.

the MIS 11 and 9 for the three southern cores (Fig. 8). The two northern cores are almost barren of coccolithophorids (Fig. 8).

The Ti/Ca ratio is one of the easiest parameters to correlate through the entire GIN seas (Fig. 9). Around 4–3 m depth in the southern cores, a succession of short positive peaks defines the MIS 6–8 according to the CAZ.

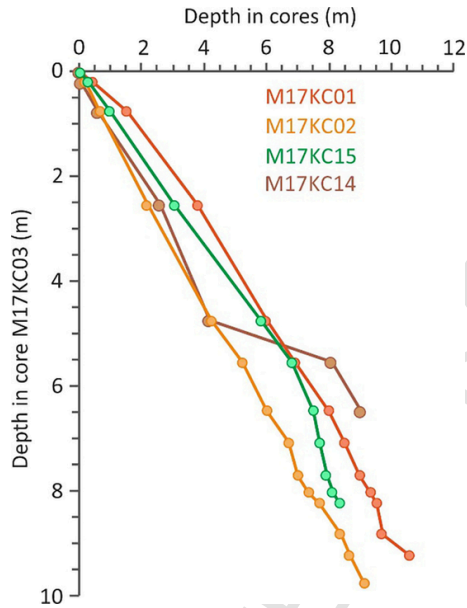

Fig. 7 Original depths in cores M17KC01, M17KC02, M17KC14 and M17KC15 with reference to their equivalent depth after their tuning with core M17KC03 using the 14 tie-points cited in Table 5.

Chapman and Shackleton (1998), Bauch et al. (2000), and Debret et al. (2011), among others, demonstrated the importance of the lightness (L*) as a paleoclimatic indicator with whitest sediments marking warmest periods and darkest sediments marking coldest ones. Here, this parameter depicts good match for the three southern cores (Fig. 10). The correlation is less obvious between the two northern cores, but the L* variations are similar. The CAZ MIS 6–8, around 4–3 m depth, presents a low L*, indicative of dark sediments, whereas the CAZ MIS 9–11, around 6 m depth in sediment, presents very high L* values, characteristic of whiter sediments.

The Sr/sum ratio parameters depict good parallelism through the southern GIN seas (Supplementary information in the online version at https://doi.org/10.1016/bs.sats.2022.09.004—Fig. SI-2). Similarly to the Ca/sum ratio, there is a high peak of Sr/sum identified around 5–7 m depth in the cores M17KC03, M17KC02, M17KC01, showing the CAZ MIS 9–11. Reversely, the CAZ MIS 8 shows low values of Sr/sum ratio. Finally, planktonic foraminifera count, in this article depicted by their absolute abundances in the sediment (number of specimens per gram of

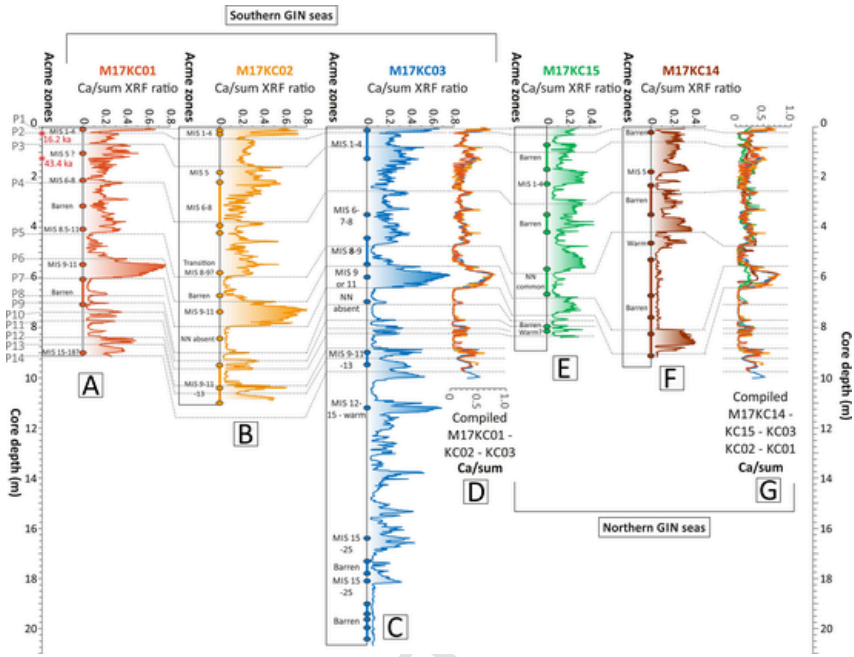

Fig. 8 ^{XRF}Ca/sum records from the five MOCO17 sedimentary cores (presented in depth) along a south-north gradient. Correlation (dashed lines) are based on the 14 tie-points (P1–P14) listed on the left of the figure and in Table 5. The coccolithophorids acme zones (CAZ) are presented on the left side of each curve. (A) ^{XRF}Ca/sum in M17KC01 (red curve). (B) ^{XRF}Ca/sum ratio M17KC02 (orange curve). (C) ^{XRF}Ca/sum ratio in M17KC03 (blue curve, reference curve). (D) Stacked ^{XRF}Ca/sum ratio in cores M17KC01, M17KC02 and M17KC03 vs. core depth in reference core M17KC03. (E) ^{XRF}Ca/sum ratio in M17KC15 (green curve). (F) ^{XRF}Ca/sum ratio in M17KC14 (brown curve). (G) Stacked ^{XRF}Ca/sum ratio in the five MOCO17 sedimentary cores vs. core depth in reference core M17KC03.

dried sed.), reveal a very good regional consistency (Supplementary information in the online version at https://doi.org/10.1016/bs.sats.2022.09.004—Fig. SI-3). Some coherent peaks are identified through the southern cores. Around 2–1 m depth in the sediment, a positive peak is dated from MIS 5 according to the CAZ, and the strongest abundance peak, around 6 m depth, marks the CAZ MIS 9–11.

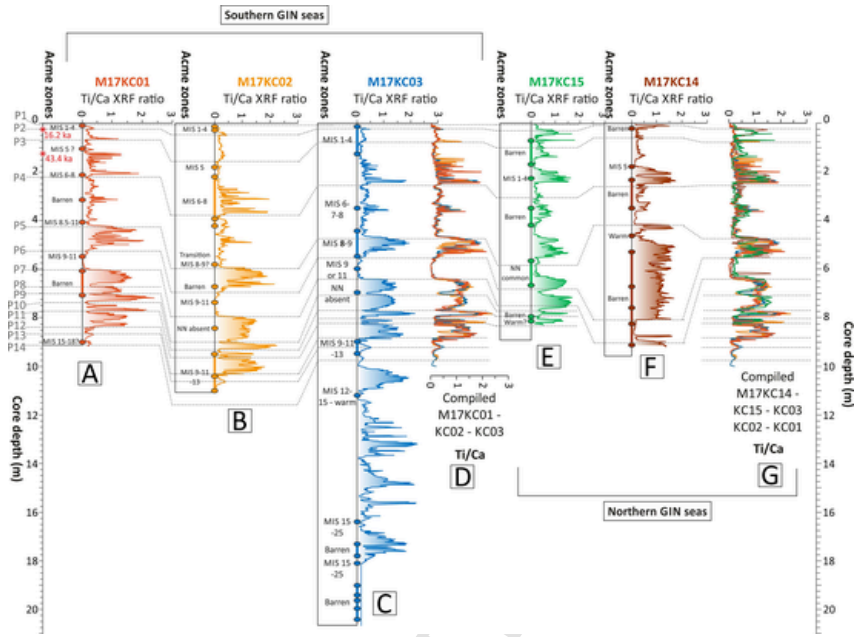

Fig. 9 $^{XRF}Ti/^{XRF}Ca$ ratio records from the five MOCO17 sedimentary cores (presented in depth) along a south-north gradient. Correlation (dashed lines) are based on the 14 tie-points (P1–P14) listed on the left of the figure and in Table 5. The coccolithophorids acme zones (CAZ) are presented on the left side of each curve. (A) $^{XRF}Ti/^{XRF}Ca$ ratio in M17KC01 (red curve). (B) $^{XRF}Ti/^{XRF}Ca$ ratio in M17KC02 (orange curve). (C) $^{XRF}Ti/^{XRF}Ca$ ratio in M17KC03 (blue curve, reference curve). (D) Stack $^{XRF}Ti/^{XRF}Ca$ ratio in cores M17KC01, M17KC02 and M17KC03 vs. core depth in reference core M17KC03. (E) $^{XRF}Ti/^{XRF}Ca$ ratio in M17KC15 (green curve). (F) $^{XRF}Ti/^{XRF}Ca$ ratio in M17KC14 (brown curve). (G) Stack $^{XRF}Ti/^{XRF}Ca$ ratio in the five MOCO17 sedimentary cores vs. core depth in reference core M17KC03.

4. Discussion

4.1 Coherent stratigraphy over GIN seas

The studied cores have been correlated on the basis of the age model first established on the core M17KC03 (Figs. 12–14), providing the depositional history over the last 500 ka BP, thus since the end of the Mid-Pleistocene Transition (MPT).

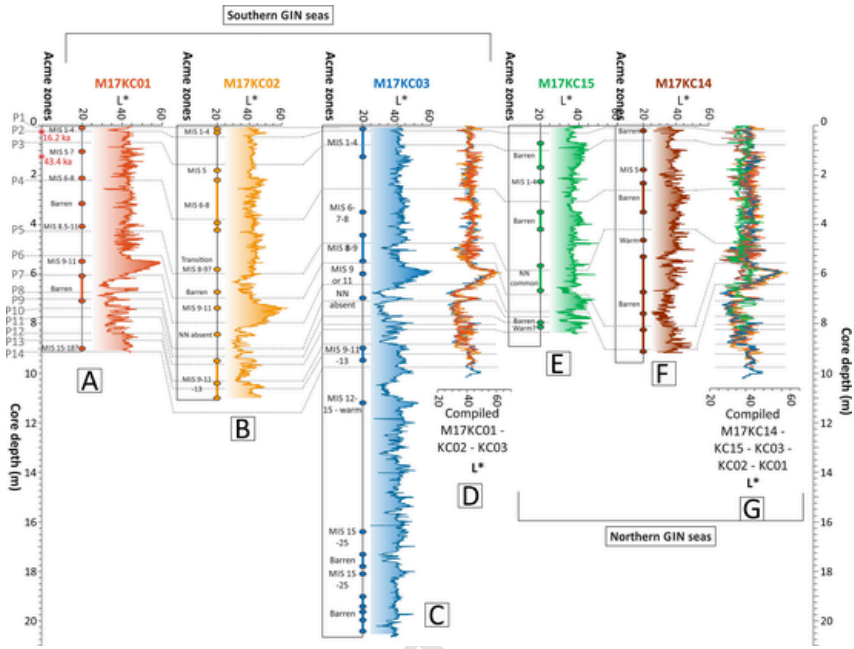

Fig. 10 Lightness L* records from the five MOCO17 sedimentary cores (presented in depth) along a south-north gradient. Correlation (dashed lines) are based on the 14 tie-points (P1–P14) listed on the left of the figure and in Table 5. The coccolithophorids acme zones (CAZ) are presented on the left side of each curve. (A) Lightness L* in M17KC01 (red curve). (B) Lightness L* in M17KC02 (orange curve). (C) Lightness L* in M17KC03 (blue curve, reference curve). (D) Compilation of the three firsts sedimentary s (M17KC01, M17KC02 and M17KC03) presented here in correlated depth. (E) Lightness L* in M17KC15 (green curve). (F) Lightness L* in M17KC14 (brown curve). (G) Stack L* in the five MOCO17 sedimentary cores vs. core depth in reference core M17KC03.

The comparison of the multiproxy record during this time interval reveals strong regional patterns with typical signatures over glacials (G) as well as terminations (T) and interglacials (IG), worth to be noted here as potential stratigraphical landmarks in the GIN seas. The pulses of sedimentation rates during terminations are synchronous with maximum of obliquity and summer and winter insolation at 65°N (Fig. 11). A latitudinal gradient is observed in the Ti/Ca and Sr/Ca ratio with northern records being much more imprinted by such high values during the nearly complete duration of glacials (Fig. 12B and D). The possible causality of such a sedimentary specificity in the GIN seas will be dis-

Table 5 Tie-points used for correlating M17KC03 with the four other MOCOSED 2017 cores.

	Reference Core		Correlated cores		
	M17KC03	**M17KC01**	**M17KC02**	**M17KC14**	**M17KC15**
Pointers	Core depth (m from top)	Core depth (m from top)	Core depth (m from top)	Core depth (m from top)	Core depth (m from top)
1	0.04	0.04	0.04	0.00	0.04
2	0.23	0.21	0.47	0.04	0.31
3	0.79	0.67	1.56	0.10	1.00
4	2.56	2.19	3.80	0.60	3.06
5	4.75	4.26	6.00	2.60	5.83
6	5.55	5.26	6.92	4.19	6.82
7	6.47	6.04	8.01	8.10	7.51
8	7.08	6.72	8.51	9.05	7.72
9	7.70	7.01	9.01		7.94
10	8.03	7.38	9.34		8.14
11	8.23	7.73	9.56		8.35
12	8.82	8.39	9.73		
13	9.22	8.67	10.61		
14	9.75	9.14			

cussed in details (Section III.4.2), taking into account other pan-Atlantic similar long records and potential forcings.

Over the last 1000 ka BP, each IG records evidences of highest positive excursions in the set of selected parameters we have used for correlation (Figs. 11–13). The main outstanding and coherent feature for the investigated IG is their record of signatures typifying a dominant calcareous content (obvious with all related indices, i.e.: Ca/sum, Ca/Sr, L* for the entire GIN seas and Sr/sum, Ti/Ca, Sr/Ti, and absolute concentrations of foraminifera for the southern GIN seas, Figs. 12 and 13). A gradient is clearly expressed in the set of cores we have used, with more pronounced positive excursions recorded in the southern GIN seas. This feature (i.e., high calcareous amounts during IG) is of course not a surprise for subpolar basins and was at the basis of stratigraphical approaches for many cores from the northern NAtl (e.g., Carbonara et al., 2016; Helmke and Bauch, 2002; Lucchi et al., 2013). However, tie points generated for core to core correlation, if chosen on the basis of Ca proxies, were dated thanks to the crossing of the M17KC03 planktonic $\delta^{18}O$ signal compared with the LR04 and constrained by CAZ. Our findings

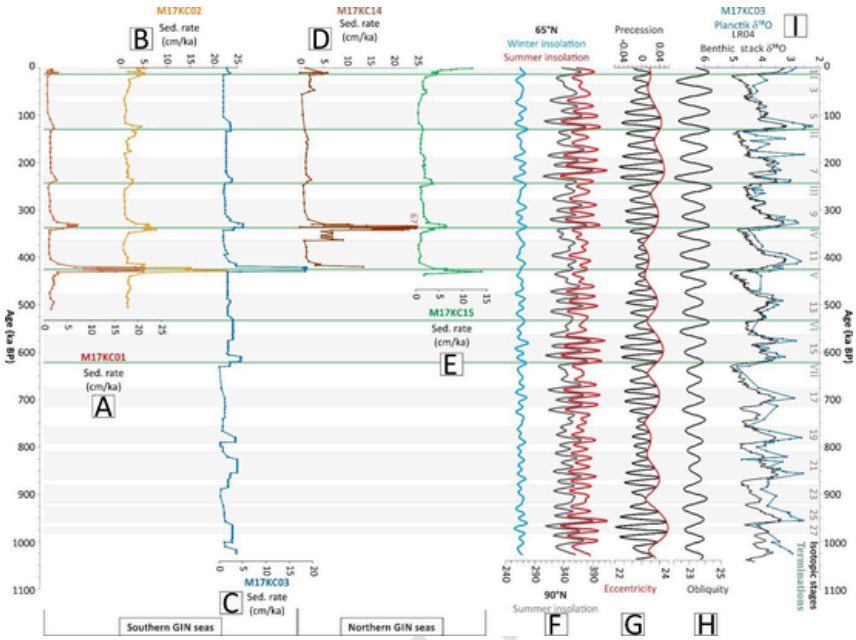

Fig. 11 Derived sedimentation rates in the five sediment cores from MOCOSED 2017 along a south-north gradient. (A) in M17KC01. (B) in M17KC02. (C) in M17KC03. (D) in M17KC14. (E) in M17KC15. They are put in the frame of the: (F) Winter insolation at 65°N (light blue curve, from Laskar et al., 2004) and summer insolation at 65°N and 90°N (respectively red curve and dark gray curve, from Laskar et al., 2004), (G) Precession parameter (black curve) and eccentricity parameter (red curve) from Laskar et al., 2004, (H) Obliquity parameter (black curve) from Laskar et al., 2004, (I). Benthic stack LR04 (black curve) and the tuned M17KC03 planktonic $\delta^{18}O$ (light blue curve).

thus confirm a better preservation of carbonates during IG, either related to enhanced carbonaceous pelagic production, and/or minored dissolution processes as well.

Each IG is however strictly different from the other and some high values occur also at IG/G transitions (and G/IG conversely). At orbital scale, the Ca/sum, Ca/Sr, L*, planktonic foraminifera counting and Sr/Ti signatures recorded for MIS 9 and MIS 7 show moderate excess in amplitude in comparison to MIS 11 and 5 (Figs. 12 and 13). This variation in the amplitude probably reflects some kind of threshold in the warming intensities, necessary to generate a better preservation of carbonates (e.g., Helmke and Bauch, 2002; Huber et al., 2000). The modulation of the amplitude from a MIS to another echoes observations done in compara-

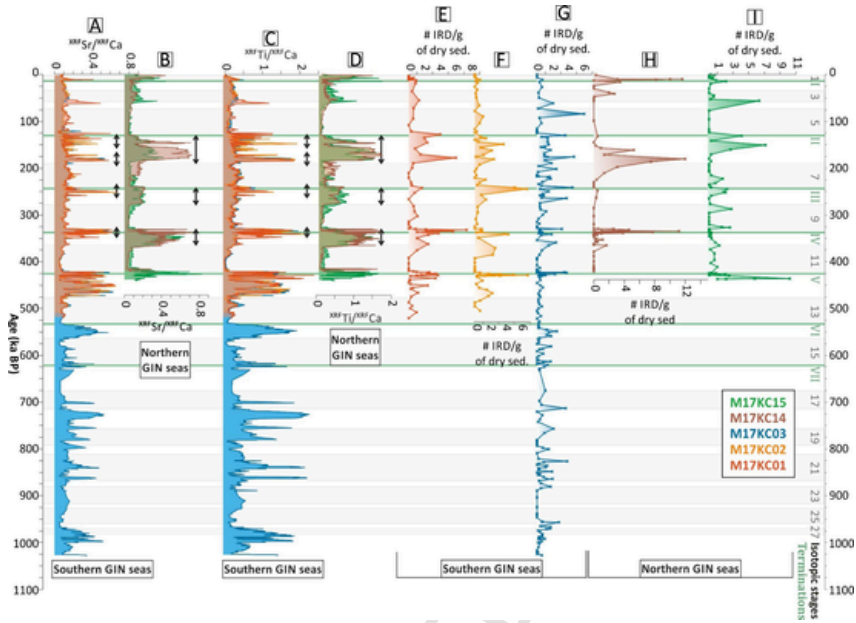

Fig. 12 Multiproxy compilation for the five MOCOSED 2017 sedimentary cores in age. (A) Southern cores $^{XRF}Sr/^{XRF}Ca$ compilation. (B) Northern cores $^{XRF}Sr/^{XRF}Ca$ compilation. (C) Southern cores $^{XRF}Ti/^{XRF}Ca$ compilation. (D) Northern cores $^{XRF}Ti/^{XRF}Ca$ compilation. Those data are compared to the IRD counts (number per gram of dry sediment) for each respective core: (E) M17KC01, (F) M17KC02, (G) M17KC03, (H) M17KC14, (I) M17KC15.

ble long records from the proximal Atlantic (Channell et al., 2012). Interestingly, in the GIN sediments, except for the sedimentation rate rises (Fig. 11), the modulation does not seem to be a direct imprint of insolation forcings (documented here by winter and summer values at 65°N, and summer insolation at 90°N). No coherent pattern occurs even if for the last 500 ka BP, Ca/sum highest values (i.e., peaks, interpreted as warm events after Bauch and collaborator's works, light green bands on Fig. 13) are related to high obliquity values before 500 ka BP and rather to low ones after, and also, to low or decreasing summer insolation at 90°N and winter insolation at 65°N. This observation tends to suggest that Ca preservation/warmth peaks in the GIN seas may occur during polar conditions with limited melting during summer (with impacts on the bottom and surface circulation and on the existence of polynyas) (Kaboth-Bahr et al., 2019).

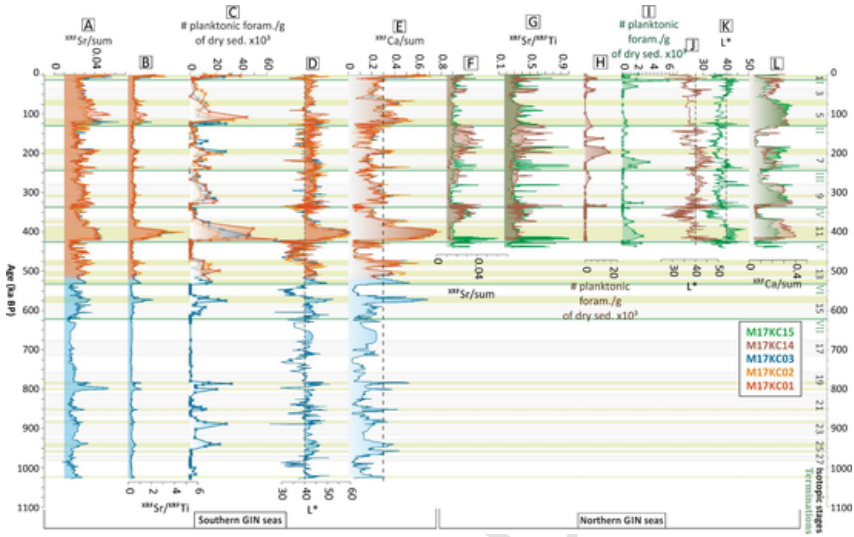

Fig. 13 Multiproxy compilation for the five MOCOSED 2017 sedimentary cores in age. (A) Southern cores ^{XRF}Sr/sum compilation. (B) Southern cores ^{XRF}Sr/^{XRF}Ti compilation. (C) Southern cores planktonic foraminifera counts compilation. (D) Southern cores lightness compilation. (E) Southern cores ^{XRF}Ca/sum compilation. (F) Northern cores ^{XRF}Sr/sum compilation. (G) Northern cores ^{XRF}Sr/^{XRF}Ti compilation. (H) M17KC14 planktonic foraminifera counts per gram of dry sediment. (I) M17KC15 planktonic foraminifera counts per gram of dry sediment. (J) M17KC14 lightness. (K) M17KC15 lightness. (L) Northern cores ^{XRF}Ca/sum compilation.

As previously introduced, Glacials are featured by high Ti/Ca, Sr/Ca values (Fig. 12A–D), and by high IRD amount (Fig. 12E–I) but again (as also seen during IG but with conversely low values), each of them depicts different ranges in the recorded amplitudes. Over the last 1000 ka BP, the most prominent signals are related to MIS 6, MIS 12 and MIS 18. The MIS 6 is known to be marked by a large geographical extension of European ice-sheets (e.g., Ehlers and Gibbard, 2007; Svendsen, 2004), MIS 12 by a very intense decay of ice-rafted material up to the Iberian margin latitudes (Ehlers and Gibbard, 2007; Kandiano et al., 2012; Rodríguez-Tovar et al., 2015), and for MIS 18, the oldest, by the lying of the Brunhes-Matuyama reversal, previous the firsts Heinrich Like Events really identified in the boreal seas (Channell et al., 2010; Naafs et al., 2013). Interestingly, the Saalian glaciation attributed to MIS 6 has been suggested by modeling exercises (Colleoni et al., 2016), following geological evidences on the sea-floor (e.g., Hughes et

al., 1977; Jakobsson et al., 2010, 2016), to be characterized by one of the largest extensions of boreal ice-shelves over the Arctic domain. Few constrains exist on the dimension of MIS 12 ice-sheets (related to the Elsterian/Anglian glaciation) but evidences of large terrigenous advection to the boreal Atlantic have already been documented, and this period has been described as one of the most severe Glacials of the Quaternary (Koutsodendris et al., 2019; Toucanne et al., 2009; Wagner et al., 2017). The data presented in this paper suggest major changes and reorganizations in the drainage configuration of boreal ice-sheets at that time, potentially calling for mechanistic effects related to a post-MPT period, initiated with MIS 16, after which Heinrich events began to appear under a context of largest thickness of ice-sheets and glacial durations (Hodell et al., 2008; Naafs et al., 2013). We could thus make an extrapolation in the interpretations and suggest that Ti/Ca and Sr/Ca values -associated to high amount of IRD in the GIN seas are proportional to the boreal ice-sheet sizes and/or decay modes. This latter extrapolation is coherent with the regolith layer hypothesis (Willeit et al., 2019) which supports a change in the intensity and modality of glacial erosion after MIS 18.

If we detect some coherent timings of Ti/Ca high values from a core to another, peaks are however not perfectly synchronously recorded and some appear to be isolated on specific intervals (Fig. 12C and D). This is especially the case when comparing the northern and southern basins, as for instance during glacial terminations. Termination IV, before MIS 9, is restricted to a narrow time period in the southern basin in comparison to what is recorded for northern records. Does this observation sign continuous terrigenous advections (from ice-sheets) during MIS 10 in the north whereas it does occur more briefly in the south? Or following the argumentation of Hodell et al. (2008) for the initiation of Heinrich events, does it mean that glacial purges are related to critical thresholds in the size of ice-sheets (or even ice-shelves?), and thus that northern glaciers were thicker, as proposed by Hughes et al. (1977) and Jakobsson et al. (2016)?

4.2 The GIN seas at orbital scales: Forcings, teleconnections and typicity?

The temporal cover of our study, which thanks to core M17KC03, extends over 1000 ka BP with no detected major gap, offers the possibility to test teleconnections existing in between the GIN seas and the changes at hemispheric and global scales. Over the last decade, long and well-re-

solved records, covering the MPT at least, have been produced in several basin of the NAtl and worldwide. Even if the comparison is sometime hampered by stratigraphical issues, changes marking the last 22 marine isotopic stages can be discussed robustly when limiting our observations to plurimillennial trends. We have thus selected some records along a latitudinal gradient from the tropics to the temperate belt to tentatively identify forcings driving the modulation of the recorded signals in the GIN seas, with a focus on the calcareous sedimentation especially. Fig. 14 thus compiles those records, together with the EPICA dome C methane record, the latter being considered as representing a global signal, thanks to the short residence time of the greenhouse gas in the atmosphere, and furthermore coeval with changes in the hydrological budget in spite of diversified sources (e.g., Landais et al., 2005; Parrenin et al., 2012, 2013, 2015, 2017; Tzedakis et al., 2006, 2009; and reference therein).

This compilation highlights striking phasing when considered the Ca peaks (values of the ratio Ca/sum overpassing 0.3 in the GIN seas, see pink bands on Fig. 14 and light green bands on Fig. 13), suggesting that not only our constructed age scales are robust, but also that recorded changes really traduce pan-Atlantic modulations with warmings detected in the GIN seas corresponding to global warmings and pulses of high methane atmospheric contents. This latter observation could be in favor of a strong link in between boreal ice-sheet retreats and methane source changes, already observed at the scale of Heinrich events (e.g., Tzedakis et al., 2006, 2009). One very interesting result is the strong correlation of the calcium excursions detected in our records with the percentage of biogenic silica registered in the Lake Baikal (Fig. 14I and J, Prokopenko et al., 2006). In between MIS 14 and MIS 1, nearly all the peaks of Ca detected echo maxima of Ca content in other southern records and occur during IG. The discrimination is less obvious in the tropical records where a continuous pelagic and planktonic production of carbonate does occur. The combination of detrital carbonates to the Ca signal is especially expected in the Ruddiman belt (Bond et al., 1993; Hemming et al., 2002; Hodell et al., 2008; McCave and Andrews, 2019; Ruddiman and McIntyre, 1981), thus potentially affecting the MD01-2448 record, but regarding the GIN seas, our observations tend to infer an overprint from the biogenic carbonate production. Currently, detrital Ca sources around the GIN basins are restricted to North-East Greenland and Siberia areas (Andrews et al., 2017; Spencer et al.,

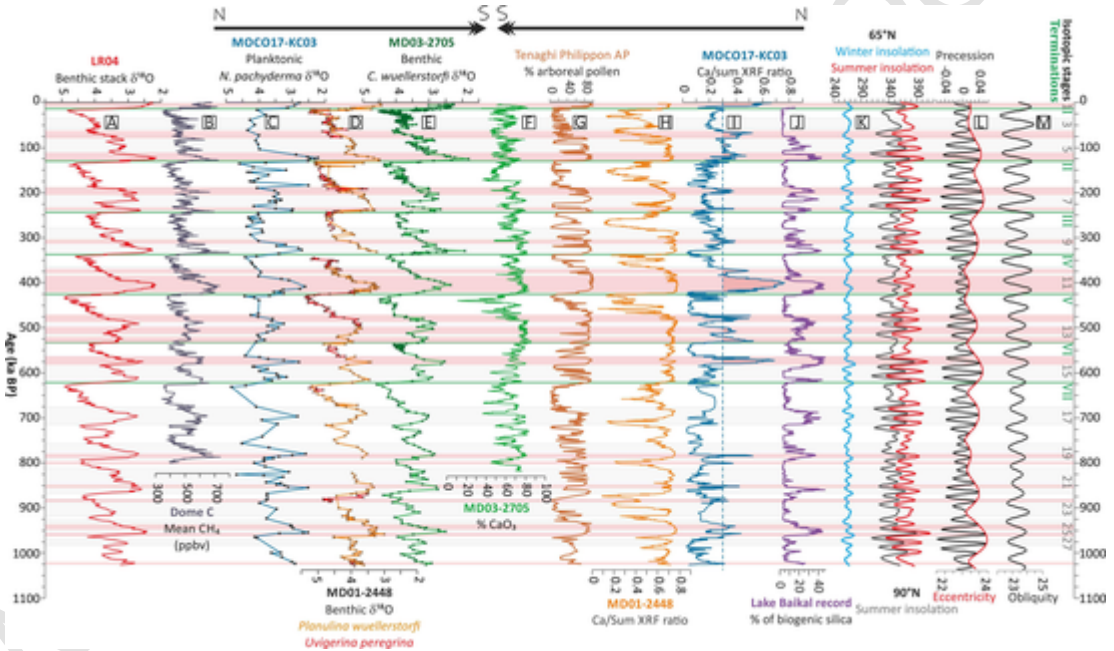
N
S
S
N
LR04
Benthic stack δ18O
MD01-2448
Benthic δ18O
Planulina wuellerstorfi
Uvigerina peregrina
MD03-2705
Benthic
C. wuellerstorfi δ18O
MD03-2705
% CaO3
MD01-2448
Ca/Sum XRF ratio
MOCO17-KC03
Planktonic
N. pachyderma δ18O
MOCO17-KC03
Ca/sum XRF ratio
Tenaghi Philippon AP
% arboreal pollen
Dome C
Mean CH4
(ppbv)
65°N
Winter insolation
Summer insolation
Precession
90°N
Summer insolation
Eccentricity
Obliquity
Lake Baikal record
% of biogenic silica
Age (ka BP)
Isotopic stages
Terminations
A
B
C
D
E
F
G
H
I
J
K
L
M

2011). However, Sr/Ca ratios correlates well with the Ti/Ca ones (Fig. 12). The correlation between Ti/Ca and Sr/Ca can be explained by the enhanced detrital/continental supplies which dilute partially the bio-productivity and thus the link between calcium and strontium. In the northern GIN seas, the reduced primary production coupled to the vicinity of Greenland and Svalbard are responsible of the same mechanism to a larger scale: the Sr in calcareous foraminifera is invisible in the sediment, making only the detrital Sr as a marker in the sediment. This explains the two different patterns showed by Sr/sum ratio values during interglacials for the last 500 ka BP: a positive correlation with the Ca/sum peaks, thus to biogenic production, in the southern GIN seas (Fig. 3A–E); and a negative correlation between those parameters in the northern GIN seas (Fig. 13F–I). Moreover, high Sr amounts most probably call for a detrital source in or around the Fram Strait when ice-sheets are at their maximum extension, maybe linked with coastal related deposits thus submitted to glacier erosion. This hypothesis is corroborated in the Fig. 13 which presents a positive correlation between planktonic foraminifera

Fig. 14 Pan Atlantic comparison in between high and low latitudes records for the last 1 million years. Light gray bands correspond to interglacial periods after Lisiecki and Raymo, 2005. Pink bands correspond to M17KC03 Ca/sum ratio > 0.3. (A) $\delta^{18}O$ LR04 benthic stack (black curve, Lisiecki and Raymo, 2005). (B) Dôme C mean CH_4 values from Antarctica (ice core, EDC, 1999). (C) M17KC03 monospecific planktonic $\delta^{18}O$, GIN seas (blue curve, this study). (D) Compilation of two benthic $\delta^{18}O$ from the sedimentary core MD01-2448, Bay of Biscay, mid-latitude (orange curve for *P. wuellerstorfi*, red curves for *U. peregrina*; Toucanne et al., 2009). (E) Monospecific *P. wuellerstorfi* benthic $\delta^{18}O$ from the sedimentary core MD03-2705, west-Africa, low latitude (green curve, Malaizé et al., 2012). (F) Carbonate percentage in the core MD03-2705 west-Africa, low latitude (green curve, Malaizé et al., 2012). (G) Percentage of arboreal pollens from Greece, Tenaghi Philippon AP (Tzedakis et al., 2006). (H) Ca/sum ratio from the MD01-2448 core, Bay of Biscay, mid-latitude (yellow curve, Toucanne et al., 2009). (I) Ca/sum ratio from the M17KC03, GIN seas (blue curve, this study). (J) Percentage of biologic silica in the sediment from the Lake Baikal (Prokopenko et al., 2006). (K) Winter insolation at 65°N (light blue curve, from Laskar et al., 2004) and summer insolation at 65°N and 90°N (respectively red curve and dark gray curve, from Laskar et al., 2004). (L) Precession parameter (black curve) and eccentricity parameter (red curve) from Laskar et al., 2004. (M) Obliquity parameter (black curve) from Laskar et al., 2004.

amount in the southern GIN seas and Sr/Ti ratio. This correlation exists in the northern GIN seas, but with a very little amplitude, implying rather a detrital source for the Sr.

Interestingly, carbonate excursions in the GIN seas were previously related to IG rather to G (Helmke and Bauch, 2002). The latter authors noted enhanced carbonate dissolution during IG in relation to more productive sea-surface waters which in return conducted to more aggressive corrosion processes at the bottom. Their observations were especially well illustrated with MIS 11, with a high index of weight loss for *N. pachyderma* shells noted for cores retrieved in the vicinity of the Jan Mayen Island. Surprisingly using the same and other proximal marine archives, they also observed a high Ca content during MIS 11 (e.g., Helmke et al., 2005; Helmke and Bauch, 2002; Kandiano et al., 2012, 2016, 2017), similarly to what we have observed in the M17KC03 core (Figs. 8 and 13). This "carbonate shoot" was also detected in several ODP drillings from the south-eastern GIN seas by Henrich et al. (2002), the latter author attributing this feature to "*an extraordinary high carbonate production in surface waters,*" in a post-MPT context of growing carbonate contents preserved in the youngest sediments. Further extensive works conducted by the same research group (e.g., Kandiano et al., 2012, 2016, 2017 and references therein) on the MIS 11 oceanographic conditions lead them to conclude that this stage was cooler in the GIN seas than today. They explained those lower Sea Surface Temperature (SST) values by intense and steady melting of the Greenland Ice-Sheet (GIS), even after the end of the Termination V, at 420 ka BP. This melting would imply the formation of a thick and south-western extended fresh surface water in the GIN seas, until 68°N and, at least, underlying the MD99-2277 core site at 6°W (Kandiano et al., 2012). The meltwater surface layer would favor a large-extent of winter sea-ice cover even during the MIS 11 sensu stricto (ss) (410–398 ka BP, Kandiano et al., 2012), enhancing the summer primary productivity and increasing the carbonate export to the bottom (Kandiano et al., 2012, 2016). MIS 11 is a period of high sea-level (6–9 m above the modern level, Raymo and Mitrovica, 2012) implying a larger collapse of polar ice sheets during this interglacial. Hillaire-Marcel and de Vernal (2008) and Reyes et al. (2014) also demonstrated a peculiar artifact in southern Greenland at that time: the southern GIS totally melted, allowing the development of a boreal forest according to their findings. It is interesting to note that our "carbonate shoot" maximum occurs at 406 ka

BP, during the MIS 11 ss, at the time of the highest SST recorded in the GIN seas (Kandiano et al., 2012). Our study thus validates their model with a large delay before the onset of the MIS 11 ss and the development of a high primary productivity in the GIN seas. All those observations converge to make MIS 11 a key period regarding climate modulations within the boreal basins: a change does happen in the water column which favored a better preservation of carbonates at that time and during recent IG. Further works focusing on that period are obviously needed in the GINS seas to better document what can be the consequences of a long interglacial in those reactive areas.

5. Conclusions

Our study allowed the determination of a coherent stratigraphic framework for recent sediments (last 500 ka BP at least) over the whole GIN seas. We demonstrated that taking into account the same systematic series of proxies, age scales can be constructed robustly. In those polar basins which suffer from low sedimentation rates and carbonate dissolution, the planktonic $\delta^{18}O$ can, but not solely, be used to generate age control points: it should be used in combination with additional proxies, especially elemental ratios obtained after XRF core-scanning and the stratigraphical control of coccolithophore acme zones are recommended tools. Correlation to the benthic stack LR04, followed by a core-to-core extrapolation, revealed coherent patterns in the sedimentation of the GIN seas at orbital scales: interglacials vs. glacials are clearly modulated at least along the last 1000 ka BP by cryospheric-oceanic-climatic tight interactions and their signals can even be linked to the middle and low latitude similarly long archives, showing a good match in the global climatic teleconnections between high and lower latitudes.

The sedimentation rates obtained from the stratigraphical framework highlight the Terminations by recording sharp rises, and especially for the Termination V which presents the strongest sedimentation rates (around 19 cm/ka) of the whole record from north to south.

Thanks to the set of studied cores distributed in the GIN seas from the south-eastern Jan Mayen plateau to the Fram strait, we have identified a N-S gradient over the last common history of our archives, i.e., over 500 ka BP, with more intense glacial conditions in the northern GIN seas than in the southern GIN seas (especially expressed throughout XRF ra-

tios and those implying the Titanium). In the same way, we have noted a deconvolution of the Sr and Ca signals in the sediment with, for the southern GIN seas, the Sr which seems to be linked to the Ca and the biogenic production, whereas in the northern GIN seas, the Sr is dissociated from the Ca and planktonic foraminifera, but presents a ratio around 1 with the Ti, giving a more detrital origin of the northern Sr.

The interglacial MIS 11 is quite peculiar in the southern GIN seas. Indeed, it is strongly highlighted by the biogenic signals, making this warm period the most prominent of the last 1000 ka BP. Interestingly, at 406 ka BP, a huge carbonate spike is recorded in the cores, during the MIS 11 sensu stricto, recognized with full-interglacial conditions in the northern hemisphere, and with an extended winter sea-ice cover in the GIN seas (Kandiano et al., 2012, 2016). Conversely, in the northern GIN seas, this very warm interglacial is under-represented, implying different N-S oceanographic conditions and processes, explained by the different vicinity of the ice-front. Those features make this warm period a very interesting one to investigate further in the GIN seas for future studies.

The two glacials MIS 12 and MIS 6 are particularly prominent in our cores. Those stages are already known as intense glacials, with very extended ice-sheets over Europe and North America, and with some proof of ice-streams extension over the Arctic Ocean (Jakobsson et al., 2016; Koutsodendris et al., 2019; Wagner et al., 2017). Our data strongly support those arguments because of the intense terrigenous discharges associated to those glacials, interpreted as the result of the high amount of detrital material produced by the extremely extended ice-sheets.

Acknowledgments

The authors are grateful to the Service Hydrographique et Océanographique de la Marine (SHOM) for funding this study. We thank GENAVIR and the crew of the R/V Pourquoi Pas? for their assistance during the cruises MOCOSED 2014 and MOCOSED 2017. We are grateful to P. Lebleu, S. Bujan, B. Martin, M-C. Perello, O. Ther, L. Devaux, M-H. Castera, A. Cogné, and M. Sabourdy for their technical assistance.

Referees suggested

Bylinskaya Marine E., because she works with similar proxies and in the same area.
Saint Onge Guillaume, because he works with similar proxies and in the same area.
Hodell David, for his expertise in stratigraphy.
Chauhan Teena, because she works with similar proxies and in the same area.
Obrochta Stephen, because he works with similar proxies and in the same area.
Laberg Jan Sverre, because he works with similar proxies and in the same area.
Knies Jochen, because he works with similar proxies and in the same area.

References

Amundsen, H.B., Laberg, J.S., Vorren, T.O., Haflidason, H., Forwick, M., Buhl-Mortensen, P., 2015. Late Weichselian–Holocene evolution of the high-latitude Andøya submarine Canyon, North-Norwegian continental margin. Mar. Geol. 363, 1–14. doi:10.1016/j.margeo.2015.02.002.

Andrews, J., 2000. Icebergs and iceberg rafted detritus (IRD) in the North Atlantic: facts and assumptions. Oceanography 13, 100–108. doi:10.5670/oceanog.2000.19.

Andrews, J.T., Dunhill, G., Vogt, C., Voelker, A.H.L., 2017. Denmark Strait during the late glacial maximum and marine isotope stage 3: sediment sources and transport processes. Mar. Geol. 390, 181–198. doi:10.1016/j.margeo.2017.07.003.

Baeten, N.J., Laberg, J.S., Vanneste, M., Forsberg, C.F., Kvalstad, T.J., Forwick, M., Vorren, T.O., Haflidason, H., 2014. Origin of shallow submarine mass movements and their glide planes-sedimentological and geotechnical analyses from the continental slope off northern Norway: glide plane of a shallow mass movement. Case Rep. Med. 119, 2335–2360. doi:10.1002/2013JF003068.

Bauch, H.A., Erlenkeuser, H., Helmke, J.P., Struck, U., 2000. A Paleoclimatic Evaluation of Marine Oxygen Isotope Stage 11 in the High-Northern Atlantic žNordic Seas/13.

Becker, L.W.M., Sejrup, H.P., Hjelstuen, B.O., Haflidason, H., Dokken, T.M., 2018. Ocean-ice sheet interaction along the SE Nordic seas margin from 35 to 15 ka BP. Mar. Geol. 402, 99–117. doi:10.1016/j.margeo.2017.09.003.

Blindheim, J., Borovkov, V., Hansen, B., Malmberg, S.-A., Turrell, W.R., Østerhus, S., 2000. Upper layer cooling and freshening in the Norwegian Sea in relation to atmospheric forcing. Deep Sea Res Part I Oceanogr. Res. Pap. 47, 655–680. doi:10.1016/S0967-0637(99)00070-9.

Bond, G.C., Devlin, W.J., Kominz, M.A., Beavan, J., McManus, J., 1993. Evidence of astronomical forcing of the earth's climate in Cretaceous and Cambrian times. Tectonophysics 222, 295–315. doi:10.1016/0040-1951(93)90356-O.

Broecker, W.S., Bond, G., Klas, M., Bonani, G., Wolfli, W., 1990. A salt oscillator in the glacial Atlantic? 1. The concept. Paleoceanography 5, 469–477. doi:10.1029/PA005i004p00469.

Bylinskaya, M.E., Golovina, L.A., Radionova, E.P., Pokrovskii, B.G., Lavrushin, V.Y., 2016. Paleoenvironments in the Fram Strait during marine isotope stages 2–6 based on planktonic paleobiological and stable-isotope proxies and ice-rafted debris. Quat. Int. 420, 272–279. doi:10.1016/j.quaint.2015.09.086.

Carbonara, K., Mezgec, K., Varagona, G., Musco, M.E., Lucchi, R.G., Villa, G., Morigi, C., Melis, R., Caffau, M., 2016. Palaeoclimatic changes in Kveithola, Svalbard, during the late Pleistocene deglaciation and Holocene: evidences from microfossil and sedimentary records. Palaeogeogr. Palaeoclimatol. Palaeoecol. 463, 136–149. doi:10.1016/j.palaeo.2016.10.003.

Caricchi, C., Sagnotti, L., Campuzano, S.A., Lucchi, R.G., Macrì, P., Rebesco, M., Camerlenghi, A., 2020. A refined age calibrated paleosecular variation and relative paleointensity stack for the NW Barents Sea: implication for geomagnetic field behavior during the Holocene. Quat. Sci. Rev. 229, 106133. doi:10.1016/j.quascirev.2019.106133.

Channell, J.E.T., Hodell, D.A., 2013. Magnetic signatures of Heinrich-like detrital layers in the quaternary of the North Atlantic. Earth Planet. Sci. Lett. 369–370, 260–270. doi:10.1016/j.epsl.2013.03.034.

Channell, J.E.T., Hodell, D.A., Singer, B.S., Xuan, C., 2010. Reconciling

astrochronological and 40 Ar/39 Ar ages for the Matuyama-Brunhes boundary and late Matuyama Chron: MATUYAMA-BRUNHES REVERSAL AGES. Geochem. Geophys. Geosyst. 11. doi:10.1029/2010GC003203.

Channell, J.E.T., Hodell, D.A., Romero, O., Hillaire-Marcel, C., de Vernal, A., Stoner, J.S., Mazaud, A., Röhl, U., 2012. A 750-kyr detrital-layer stratigraphy for the North Atlantic (IODP sites U1302–U 1303, orphan knoll, Labrador Sea). Earth Planet. Sci. Lett. 317–318, 218–230. doi:10.1016/j.epsl.2011.11.029.

Chapman, M.R., Shackleton, N.J., 1998. What level of resolution is attainable in a deep-sea core? Results of a spectrophotometer study. Paleoceanography 13, 311–315. doi:10.1029/98PA01067.

Chauhan, T., Rasmussen, T.L., Noormets, R., Jakobsson, M., Hogan, K.A., 2014. Glacial history and paleoceanography of the southern Yermak plateau since 132 ka BP. Quat. Sci. Rev. 92, 155–169. doi:10.1016/j.quascirev.2013.10.023.

Chauhan, T., Rasmussen, T.L., Noormets, R., 2016. Palaeoceanography of the Barents Sea continental margin, north of Nordaustlandet, Svalbard, during the last 74 ka. Boreas 45, 76–99. doi:10.1111/bor.12135.

Clark, P.U., Archer, D., Pollard, D., Blum, J.D., Rial, J.A., Brovkin, V., Mix, A.C., Pisias, N.G., Roy, M., 2006. The middle Pleistocene transition: characteristics, mechanisms, and implications for long-term changes in atmospheric pCO2. Quat. Sci. Rev. 25, 3150–3184. doi:10.1016/j.quascirev.2006.07.008.

Colleoni, F., Kirchner, N., Niessen, F., Quiquet, A., Liakka, J., 2016. An east Siberian ice shelf during the late Pleistocene glaciations: numerical reconstructions. Quat. Sci. Rev. 147, 148–163. doi:10.1016/j.quascirev.2015.12.023.

Debret, M., Sebag, D., Desmet, M., Balsam, W., Copard, Y., Mourier, B., Susperrigui, A.-S., Arnaud, F., Bentaleb, I., Chapron, E., Lallier-Vergès, E., Winiarski, T., 2011. Spectrocolorimetric interpretation of sedimentary dynamics: the new "Q7/4 diagram". Earth Sci. Rev. 109, 1–19. doi:10.1016/j.earscirev.2011.07.002.

Duplessy, J.-C., Shackleton, N.J., Matthews, R.K., Prell, W., Ruddiman, W.F., Caralp, M., Hendy, C.H., 1984. d13C record of benthic foraminifera in the last Interglacial Ocean: implications for the carbon cycle and the global deep water circulation. Quatern. Res. 21, 225–243. doi:10.1016/0033-5894(84)90099-1.

Ehlers, J., Gibbard, P.L., 2007. The extent and chronology of Cenozoic global glaciation. Quat. Int. 164–165, 6–20. doi:10.1016/j.quaint.2006.10.008.

Eldholm, O., Thiede, J., Taylor, E., 1987. Evolution of the Norwegian Continental Margin: Background and Objectives. p. 21.

Gkinis, V., Simonsen, S.B., Buchardt, S.L., White, J.W.C., Vinther, B.M., 2014. Water isotope diffusion rates from the NorthGRIP ice core for the last 16, 000 years—glaciological and paleoclimatic implications. Earth Planet. Sci. Lett. 405, 132–141. doi:10.1016/j.epsl.2014.08.022.

Haflidason, H., de Alvaro, M.M., Nygard, A., Sejrup, H.P., Laberg, J.S., 2007. Holocene sedimentary processes in the Andøya canyon system, North Norway. Mar. Geol. 246, 86–104. doi:10.1016/j.margeo.2007.06.005.

Heaton, T.J., Köhler, P., Butzin, M., Bard, E., Reimer, R.W., Austin, W.E.N., Bronk Ramsey, C., Grootes, P.M., Hughen, K.A., Kromer, B., Reimer, P.J., Adkins, J., Burke, A., Cook, M.S., Olsen, J., Skinner, L.C., 2020. Marine20—the marine radiocarbon age calibration curve (0–55,000 cal BP). Radiocarbon 62, 779–820. doi:10.1017/RDC.2020.68.

Helmke, J.P., Bauch, H.A., 2002. Glacial–interglacial carbonate preservation records in

the Nordic seas. Global Planet. Change 33, 15–28. doi:10.1016/S0921-8181(02)00058-9.

Helmke, J.P., Schulz, M., Bauch, H.A., 2002. Sediment-color record from the Northeast Atlantic reveals patterns of millennial-scale climate variability during the past 500,000 years. Quatern. Res. 57, 49–57. doi:10.1006/qres.2001.2289.

Helmke, J.P., Bauch, H.A., Röhl, U., Mazaud, A., 2005. Changes in sedimentation patterns of the Nordic seas region across the mid-Pleistocene. Mar. Geol. 215, 107–122. doi:10.1016/j.margeo.2004.12.006.

Hemming, S.R., Vorren, T.O., Kleman, J., 2002. Provinciality of ice rafting in the North Atlantic: application of 40Ar/39Ar dating of individual ice rafted hornblende grains. Quat. Int. 95–96, 75–85. doi:10.1016/S1040-6182(02)00029-0.

Henrich, R., Baumann, K.-H., Huber, R., Meggers, H., 2002. Carbonate preservation records of the past 3 Myr in the Norwegian–Greenland Sea and the northern North Atlantic: implications for the history of NADW production. Mar. Geol. 184, 17–39. doi:10.1016/S0025-3227(01)00279-1.

Hillaire-Marcel, C., de Vernal, A., 2008. Stable isotope clue to episodic sea ice formation in the glacial North Atlantic. Earth Planet. Sci. Lett. 268, 143–150. doi:10.1016/j.epsl.2008.01.012.

Hodell, D.A., Channell, J.E.T., Curtis, J.H., Romero, O.E., Röhl, U., 2008. Onset of "Hudson Strait" Heinrich events in the eastern North Atlantic at the end of the middle Pleistocene transition (~640 ka)?: PLEISTOCENE HEINRICH EVENTS. Paleoceanography 23. doi:10.1029/2008PA001591.

Hodell, D., Lourens, L., Crowhurst, S., Konijnendijk, T., Tjallingii, R., Jiménez-Espejo, F., Skinner, L., Tzedakis, P.C., Abrantes, F., Acton, G.D., Alvarez Zarikian, C.A., Bahr, A., Balestra, B., Barranco, E.L., Carrara, G., Ducassou, E., Flood, R.D., Flores, J.-A., Furota, S., Grimalt, J., Grunert, P., Hernández-Molina, J., Kim, J.K., Krissek, L.A., Kuroda, J., Li, B., Lofi, J., Margari, V., Martrat, B., Miller, M.D., Nanayama, F., Nishida, N., Richter, C., Rodrigues, T., Rodríguez-Tovar, F.J., Roque, A.C.F., Sanchez Goñi, M.F., Sierro Sánchez, F.J., Singh, A.D., Sloss, C.R., Stow, D.A.V., Takashimizu, Y., Tzanova, A., Voelker, A., Xuan, C., Williams, T., 2015. A reference time scale for site U1385 (Shackleton site) on the SW Iberian margin. Global Planet. Change 133, 49–64. doi:10.1016/j.gloplacha.2015.07.002.

Huber, R., Meggers, H., Baumann, K.-H., Henrich, R., 2000. Recent and Pleistocene carbonate dissolution in sediments of the Norwegian–Greenland Sea. Mar. Geol. 165, 123–136. doi:10.1016/S0025-3227(99)00138-3.

Hughes, T., Denton, G.H., Grosswald, M.G., 1977. Was there a late-Würm Arctic ice sheet? Nature 266, 596–602.

Jakobsson, M., Løvlie, R., Al-Hanbali, H., Arnold, E., Backman, J., Mörth, M., 2000. Manganese and color cycles in Arctic Ocean sediments constrain Pleistocene chronology. Geology 28, 23–26 4.

Jakobsson, M., Nilsson, J., O'Regan, M., Backman, J., Löwemark, L., Dowdeswell, J.A., Mayer, L., Polyak, L., Colleoni, F., Anderson, L.G., Björk, G., Darby, D., Eriksson, B., Hanslik, D., Hell, B., Marcussen, C., Sellén, E., Wallin, Å., 2010. An Arctic Ocean ice shelf during MIS 6 constrained by new geophysical and geological data. Quat. Sci. Rev. 29, 3505–3517. doi:10.1016/j.quascirev.2010.03.015.

Jakobsson, M., Nilsson, J., Anderson, L., Backman, J., Björk, G., Cronin, T.M., Kirchner, N., Koshurnikov, A., Mayer, L., Noormets, R., O'Regan, M., Stranne, C., Ananiev, R., Barrientos Macho, N., Cherniykh, D., Coxall, H., Eriksson, B., Flodén, T., Gemery, L., Gustafsson, Ö., Jerram, K., Johansson, C., Khortov, A., Mohammad, R.,

Semiletov, I., 2016. Evidence for an ice shelf covering the Central Arctic Ocean during the penultimate glaciation. Nat. Commun. 7, 10365. doi:10.1038/ncomms10365.

Jansen, E., Raymo, M.E., Blum, P., 1996. Site 985. In: Jansen, E., Raymo, M.E., Blum, P. (Eds.), et al., Proc. ODP, Init. Repts, 162. Ocean Drilling Program, College Station, TX, p. 33. doi:10.2973/odp.proc.ir.162.108.1996.

Kaboth-Bahr, S., Denis, V., Su, C.-C., O'Regan, M., Gyllencreutz, R., Jakobsson, M., Löwemark, L., 2019. Deciphering ~45.000 years of Arctic Ocean lithostratigraphic variability through multivariate statistical analysis. Quat. Int. 514, 141–151. doi:10.1016/j.quaint.2018.11.043.

Kandiano, E.S., Bauch, H.A., Fahl, K., Helmke, J.P., Röhl, U., Pérez-Folgado, M., Cacho, I., 2012. The meridional temperature gradient in the eastern North Atlantic during MIS 11 and its link to the ocean–atmosphere system. Palaeogeogr. Palaeoclimatol. Palaeoecol. 333–334, 24–39. doi:10.1016/j.palaeo.2012.03.005.

Kandiano, E.S., van der Meer, M.T.J., Bauch, H.A., Helmke, J., Damsté, J.S.S., Schouten, S., 2016. A cold and fresh ocean surface in the Nordic seas during MIS 11: significance for the future ocean. Geophys. Res. Lett. 43, 10,929-10,937. doi:10.1002/2016GL070294.

Kandiano, E.S., van der Meer, M.T.J., Schouten, S., Fahl, K., Sinninghe Damsté, J.S., Bauch, H.A., 2017. Response of the North Atlantic surface and intermediate ocean structure to climate warming of MIS 11. Sci. Rep. 7, 46192. doi:10.1038/srep46192.

Kissel, C., Laj, C., Lehman, B., Labyrie, L., Bout-Roumazeilles, V., 1997. Changes in the strength of the Iceland–Scotland Overflow Water in the last 200, 000 years: Evidence from magnetic anisotropy analysis of core SU90–33. Earth Planet. Sci. Lett. 152, 25–36. doi:10.1016/S0012-821X(97)00146-5.

Knies, J., Matthiessen, J., Vogt, C., Laberg, J.S., Hjelstuen, B.O., Smelror, M., Larsen, E., Andreassen, K., Eidvin, T., Vorren, T.O., 2009. The Plio-Pleistocene glaciation of the Barents Sea–Svalbard region: a new model based on revised chronostratigraphy. Quat. Sci. Rev. 28, 812–829. doi:10.1016/j.quascirev.2008.12.002.

Koutsodendris, A., Kousis, I., Peyron, O., Wagner, B., Pross, J., 2019. The marine isotope stage 12 pollen record from Lake Ohrid (SE Europe): investigating short-term climate change under extreme glacial conditions. Quat. Sci. Rev. 221, 105873. doi:10.1016/j.quascirev.2019.105873.

Laberg, J.S., Vorren, T.O., Dowdeswell, J.A., Kenyon, N.H., Taylor, J., 2000. The Andøya Slide and the Andøya Canyon, north-eastern Norwegian–Greenland Sea. Mar. Geol. 162, 259–275. doi:10.1016/S0025-3227(99)00087-0.

Landais, A., Jouzel, J., Masson-Delmotte, V., Caillon, N., 2005. Large temperature variations over rapid climatic events in Greenland: a method based on air isotopic measurements. C. R. Geosci. 337, 947–956. doi:10.1016/j.crte.2005.04.003.

Laskar, J., Correia, A.C.M., Gastineau, M., Joutel, F., Levrard, B., Robutel, P., 2004. Long term evolution and chaotic diffusion of the insolation quantities of Mars. Icarus 170, 343–364. doi:10.1016/j.icarus.2004.04.005.

Lisiecki, L.E., Raymo, M.E., 2005. A Pliocene-Pleistocene stack of 57 globally distributed benthic δ18O records. Paleoceanography 20. doi:10.1029/2004PA001071.

Lisiecki, L.E., Raymo, M.E., Curry, W.B., 2008. Atlantic overturning responses to late Pleistocene climate forcings. Nature 456, 85–88. doi:10.1038/nature07425.

Lucchi, R.G., Camerlenghi, A., Rebesco, M., Colmenero-Hidalgo, E., Sierro, F.J., Sagnotti, L., Urgeles, R., Melis, R., Morigi, C., Bárcena, M.-A., Giorgetti, G., Villa,

G., Persico, D., Flores, J.-A., Rigual-Hernández, A.S., Pedrosa, M.T., Macri, P., Caburlotto, A., 2013. Postglacial sedimentary processes on the Storfjorden and Kveithola trough mouth fans: significance of extreme glacimarine sedimentation. Global Planet. Change 111, 309–326. doi:10.1016/j.gloplacha.2013.10.008.

Martrat, B., Jimenez-Amat, P., Zahn, R., Grimalt, J.O., 2014. Similarities and dissimilarities between the last two deglaciations and interglaciations in the North Atlantic region. Quat. Sci. Rev. 99, 122–134. doi:10.1016/j.quascirev.2014.06.016.

McCave, I.N., Andrews, J.T., 2019. Distinguishing current effects in sediments delivered to the ocean by ice. I. Principles, methods and examples. Quat. Sci. Rev. 212, 92–107. doi:10.1016/j.quascirev.2019.03.031.

Müller, J., Stein, R., 2014. High-resolution record of late glacial and deglacial sea ice changes in Fram Strait corroborates ice–ocean interactions during abrupt climate shifts. Earth Planet. Sci. Lett. 403, 446–455. doi:10.1016/j.epsl.2014.07.016.

Myhre, A.M., Eldholm, O., 1988. The western Svalbard margin (74°–80°N). Mar. Pet. Geol. 5, 134–156. doi:10.1016/0264-8172(88)90019-0.

Naafs, B.D.A., Hefter, J., Stein, R., 2013. Millennial-scale ice rafting events and Hudson Strait Heinrich(−like) events during the late Pliocene and Pleistocene: a review. Quat. Sci. Rev. 80, 1–28. doi:10.1016/j.quascirev.2013.08.014.

Nagao, S., Nakashima, S., 1992. The factors controlling vertical color variations of North Atlantic Madeira abyssal plain sediments. Mar. Geol. 109, 83–94. doi:10.1016/0025-3227(92)90222-4.

Paillard, D., Labeyrie, L., Yiou, P., 1996. Macintosh program performs time-series analysis. Eos Trans. Am. Geophys. Union 77, 379. doi:10.1029/96EO00259.

Parrenin, F., Barker, S., Blunier, T., Chappellaz, J., Jouzel, J., Landais, A., Masson-Delmotte, V., Schwander, J., Veres, D., 2012. On the gas-ice depth difference (Δdepth) along the EPICA Dome C ice core. Climate Past Discuss. 8, 1089–1131. doi:10.5194/cpd-8-1089-2012.

Parrenin, F., Masson-Delmotte, V., Köhler, P., Raynaud, D., Paillard, D., Schwander, J., Barbante, C., Landais, A., Wegner, A., Jouzel, J., 2013. Synchronous change of atmospheric CO2 and Antarctic temperature during the last Deglacial warming. Science 339, 1060–1063. doi:10.1126/science.1226368.

Parrenin, F., Cavitte, M.G.P., Blankenship, D.D., Chappellaz, J., Fischer, H., Gagliardini, O., Masson-Delmotte, V., Passalacqua, O., Ritz, C., Roberts, J., Siegert, M.J., Young, D.A., 2017. Is there 1.5-million-year-old ice near Dome C, Antarctica? The Cryosphere 11, 2427–2437. doi:10.5194/tc-11-2427-2017.

Prokopenko, A.A., Hinnov, L.A., Williams, D.F., Kuzmin, M.I., 2006. Orbital forcing of continental climate during the Pleistocene: a complete astronomically tuned climatic record from Lake Baikal, SE Siberia. Quat. Sci. Rev. 25, 3431–3457. doi:10.1016/j.quascirev.2006.10.002.

Pujos, A., Giraudeau, J., 1993. Répartition des Noelaerhabdaceae (nannofossiles calcaires) dans le Quaternaire moyen et supérieur des océans Atlantique et Pacifique. Oceanol. Acta 16, 349–362.

Rahmstorf, S., 1999. Shifting seas in the greenhouse? Nature 399, 523–524.

Rahmstorf, S., 2002. Ocean circulation and climate during the past 120,000 years. Nature 419, 207–214. doi:10.1038/nature01090.

Rahmstorf, S., 2013. Thermohaline Circulation. Elsevier, pp. 737–747.

Raymo, M.E., Mitrovica, J.X., 2012. Collapse of polar ice sheets during the stage 11

interglacial. Nature 483, 453–456. doi:10.1038/nature10891.

Raymo, M.E., Jansen, E., Blum, P., Herbert, T.D. (Eds.), 1999. Proceedings of the Ocean Drilling Program, 162 Scientific Results, Proceedings of the Ocean Drilling Program. Ocean Drilling Program. doi:10.2973/odp.proc.sr.162.1999.

Reyes, A.V., Carlson, A.E., Beard, B.L., Hatfield, R.G., Stoner, J.S., Winsor, K., Welke, B., Ullman, D.J., 2014. South Greenland ice-sheet collapse during marine isotope stage 11. Nature 510, 525–528. doi:10.1038/nature13456.

Richter, T.O., van der Gaast, S., Koster, B., Vaars, A., Gieles, R., de Stigter, H.C., Haas, H.D., van Weering, T.C.E., 2006. The Avaatech XRF Core scanner: technical description and applications to NE Atlantic sediments. Geol. Soc. Lond. Spec. Publ. 267, 39–50. doi:10.1144/GSL.SP.2006.267.01.03.

Rodríguez-Tovar, F.J., Dorador, J., Martin-Garcia, G.M., Sierro, F.J., Flores, J.A., Hodell, D.A., 2015. Response of macrobenthic and foraminifer communities to changes in deep-sea environmental conditions from Marine Isotope Stage (MIS) 12 to 11 at the "Shackleton Site.". Global Planet. Change 133, 176–187. doi:10.1016/j.gloplacha.2015.08.012.

Rohling, E.J., 2013. PALEOCEANOGRAPHY, PHYSICAL AND CHEMICAL PROXIES | oxygen isotope composition of seawater. In: Encyclopedia of Quaternary Science. Elsevier, pp. 915–922. doi:10.1016/B978-0-444-53643-3.00293-4.

Rothwell, R.G., Croudace, I.W., 2015. Twenty years of XRF Core scanning marine sediments: what do geochemical proxies tell us? In: Croudace, I.W., Rothwell, R.G. (Eds.), Micro-XRF Studies of Sediment Cores. Springer, Netherlands, Dordrecht, pp. 25–102. doi:10.1007/978-94-017-9849-5_2.

Ruddiman, W.F., McIntyre, A., 1981. The mode and mechanism of the last deglaciation: oceanic evidence. Quatern. Res. 16, 125–134. doi:10.1016/0033-5894(81)90040-5.

Samtleben, C., Schafer, P., Andruleit, H., Baumann, A., Baumann, K.-H., Kohly, A., Matthiessen, J., Schrader-Ritzrau, A., Synpal Working Group, 1995. Plankton in the Norwegian-Greenland Sea: from living communities to sediment assemblages? An actualistic approach. Geol. Rundsch. 84. doi:10.1007/BF00192245.

Sejrup, H.P., Haflidason, H., Andrews, J.T., 2011. A Holocene North Atlantic SST record and regional climate variability. Quat. Sci. Rev. 30, 3181–3195. doi:10.1016/j.quascirev.2011.07.025.

Shackleton, N.J., Opdyke, N.D., 1973. Oxygen isotope and Palaeomagnetic stratigraphy of equatorial Pacific Core V28-238: oxygen isotope temperatures and ice volumes on a 10" year and 10" year scale. Quatern. Res. 39–55.

Spencer, A.M., Embry, A.F., Gautier, D.L., Stoupakova, A.V., Sørensen, K., 2011. Chapter 1 an overview of the petroleum geology of the Arctic. Geol. Soc. Lond. Mem. 35, 1–15. doi:10.1144/M35.1.

Stokes, C., Clark, C., Darby, D., Hodgson, D., 2005. Late Pleistocene ice export events into the Arctic Ocean from the M'Clure Strait ice stream, Canadian Arctic Archipelago. Global Planet. Change 49, 139–162. doi:10.1016/j.gloplacha.2005.06.001.

Stoner, J.S., Channell, J.E.T., Hillaire-Marcel, C., Kissel, C., 2000. Geomagnetic paleointensity and environmental record from Labrador Sea core MD95-2024: global marine sediment and ice core chronostratigraphy for the last 110 kyr. Earth Planet. Sci. Lett. 183, 161–177. doi:10.1016/S0012-821X(00)00272-7.

Stoner, J.S., Laj, C., Channell, J.E.T., Kissel, C., 2002. South Atlantic and North Atlantic geomagnetic paleointensity stacks (0–80ka): implications for inter-hemispheric

correlation. Quat. Sci. Rev. 21, 1141–1151. doi:10.1016/S0277-3791(01)00136-6.

Stuiver, M., Reimer, P.J., 1993. Extended 14C Data Base and revised CALIB 3.0 14C age calibration Program | Radiocarbon | Cambridge Core. Radiocarbon 35, 215–230. doi:10.1017/S0033822200013904.

Svendsen, J., 2004. Late quaternary ice sheet history of northern Eurasia. Quat. Sci. Rev. 23, 1229–1271. doi:10.1016/j.quascirev.2003.12.008.

Thibodeau, B., Bauch, H.A., Pedersen, T.F., 2017. Stratification-induced variations in nutrient utilization in the polar North Atlantic during past interglacials. Earth Planet. Sci. Lett. 457, 127–135. doi:10.1016/j.epsl.2016.09.060.

Thierstein, H.R., Geitzenauer, K.R., Molfino, B., Shackleton, N.J., 1977. Global synchroneity of late Quaternary coccolith datum levels Validation by oxygen isotopes. Geology 5 (7), 400–404.

Toucanne, S., Zaragosi, S., Bourillet, J.F., Cremer, M., Eynaud, F., Van Vliet-Lanoë, B., Penaud, A., Fontanier, C., Turon, J.L., Cortijo, E., 2009. Timing of massive 'Fleuve Manche' discharges over the last 350kyr: insights into the European ice-sheet oscillations and the European drainage network from MIS 10 to 2. Quat. Sci. Rev. 28, 1238–1256. doi:10.1016/j.quascirev.2009.01.006.

Tzedakis, P.C., Hooghiemstra, H., Pälike, H., 2006. The last 1.35 million years at Tenaghi Philippon: revised chronostratigraphy and long-term vegetation trends. Quat. Sci. Rev. 25, 3416–3430. doi:10.1016/j.quascirev.2006.09.002.

Tzedakis, P.C., Raynaud, D., McManus, J.F., Berger, A., Brovkin, V., Kiefer, T., 2009. Interglacial diversity. Nat. Geosci. 2, 751–755. doi:10.1038/ngeo660.

Wagner, B., Wilke, T., Francke, A., Albrecht, C., Baumgarten, H., Bertini, A., Combourieu-Nebout, N., Cvetkoska, A., Dapos Addabbo, M., Donders, T.H., Föller, K., Giaccio, B., Grazhdani, A., Hauffe, T., Holtvoeth, J., Joannin, S., Jovanovska, E., Just, J., Kouli, K., Koutsodendris, A., Krastel, S., Lacey, J.H., Leicher, N., Leng, M.J., Levkov, Z., Lindhorst, K., Masi, A., Mercuri, A.M., Nomade, S., Nowaczyk, N., Panagiotopoulos, K., Peyron, O., Reed, J.M., Regattieri, E., Sadori, L., Sagnotti, L., Stelbrink, B., Sulpizio, R., Tofilovska, S., Torri, P., Vogel, H., Wagner, T., Wagner-Cremer, F., Wolff, G.A., Wonik, T., Zanchetta, G., Zhang, X.S., 2017. The environmental and evolutionary history of Lake Ohrid (FYROM/Albania): interim results from the SCOPSCO deep drilling project. Biogeosciences 14, 2033–2054. doi:10.5194/bg-14-2033-2017.

Wefer, G., Berger, W.H., Richter, C. (Eds.), et al., 1998a. Proceedings of the ocean drilling program 175 initial reports. In: Proceedings of the Ocean Drilling Program. Ocean Drilling Program. doi:10.2973/odp.proc.ir.175.1998.

Wefer, G., Berger, W.H., Richter, C., Grout, S., Anderson, B., Jansen, L., Maslin, P., Pufahl, V., Christensen Giraudeau, J., Hermelin, L., Motoyama, F., Yamazaki, A., Laser, M., Wigley, M., Gorgas, C., 1998b. Explanatory notes, shipboard scientific party. In: Proc. Ocean Drill. Program Initial Rep., 175. p. 20.

Willeit, M., Ganopolski, A., Calov, R., Brovkin, V., 2019. Mid-Pleistocene transition in glacial cycles explained by declining CO2 and regolith removal | science advances. Sci. Adv. 5. doi:10.1126/sciadv.aav7337.

Further reading

Baeten, N.J., Laberg, J.S., Forwick, M., Vorren, T.O., Vanneste, M., Forsberg, C.F., Kvalstad, T.J., Ivanov, M., 2013. Morphology and origin of smaller-scale mass movements on the continental slope off northern Norway. Geomorphology 187,

122–134. doi:10.1016/j.geomorph.2013.01.008.

Parrenin, F., Paillard, D., 2012. Terminations VI and VIII (~ 530 and ~ 720 kyr BP) tell us the importance of obliquity and precession in the triggering of deglaciations. Clim. Past 8, 2031–2037. doi:10.5194/cp-8-2031-2012.

Reimer, P.J., Bard, E., Bayliss, A., Beck, J.W., Blackwell, P.G., Ramsey, C.B., Buck, C.E., Cheng, H., Edwards, R.L., Friedrich, M., Grootes, P.M., Guilderson, T.P., Haflidason, H., Hajdas, I., Hatté, C., Heaton, T.J., Hoffmann, D.L., Hogg, A.G., Hughen, K.A., Kaiser, K.F., Kromer, B., Manning, S.W., Niu, M., Reimer, R.W., Richards, D.A., Scott, E.M., Southon, J.R., Staff, R.A., Turney, C.S.M., van der Plicht, J., 2013. IntCal13 and Marine13 radiocarbon age calibration curves 0–50,000 years cal BP. Radiocarbon 55, 1869–1887. doi:10.2458/azu_js_rc.55.16947.

Rørvik, K.-L., Laberg, J.S., Hald, M., Ravna, E.K., Vorren, T.O., 2010. Behavior of the northwestern part of the Fennoscandian ice sheet during the last glacial maximum – a response to external forcing. Quat. Sci. Rev. 29, 2224–2237. doi:10.1016/j.quascirev.2010.05.022.